LBL-19921
c.2

# Lawrence Berkeley Laboratory
UNIVERSITY OF CALIFORNIA

## Materials & Molecular Research Division

To be published as Chapter 21 in **Molecular Beam Surface Scattering**, John H. Wiley and Sons, New York, NY, 1985

REACTIVE SCATTERING

M. Asscher and G.A. Somorjai

June 1985

TWO-WEEK LOAN COPY
This is a Library Circulating Copy
which may be borrowed for two weeks

LBL-19921
c.2

Prepared for the U.S. Department of Energy under Contract DE-AC03-76SF00098

## DISCLAIMER

This document was prepared as an account of work sponsored by the United States Government. While this document is believed to contain correct information, neither the United States Government nor any agency thereof, nor the Regents of the University of California, nor any of their employees, makes any warranty, express or implied, or assumes any legal responsibility for the accuracy, completeness, or usefulness of any information, apparatus, product, or process disclosed, or represents that its use would not infringe privately owned rights. Reference herein to any specific commercial product, process, or service by its trade name, trademark, manufacturer, or otherwise, does not necessarily constitute or imply its endorsement, recommendation, or favoring by the United States Government or any agency thereof, or the Regents of the University of California. The views and opinions of authors expressed herein do not necessarily state or reflect those of the United States Government or any agency thereof or the Regents of the University of California.

LBL-

6/20/85

# Chapter 21: Reactive Scattering

M. Asscher

Department of Physical Chemistry and

The Fritz Haber Research Center for Molecular Dynamics

The Hebrew University of Jerusalem

Jerusalem 91904, Israel

and

G.A. Somorjai

Materials and Molecular Research Division

Lawrence Berkeley Laboratory and Department of Chemistry

University of California

Berkeley, CA 94720, U.S.A.

## Table of Contents

21.1 - Introduction

21.2 - Methods

21.2.1 - Scattering Chamber

21.2.2 - Beam Sources

21.2.3 - Data Analysis

21.3 - Reactive Scattering: Effusive Beam Sources

21.3.1 - $H_2$-$D_2$ Exchange and Recombination Reactions

21.3.2 - CO Oxidation

21.3.3 - Highly Reactive Beams

21.4 - Reactive Scattering: Supersonic Beams

21.4.1 - Activated Dissociative Adsorption and Associative Desorption

21.4.2 - Complex Surface Reactions: Products' Energy and Angular Distributions

21.4.3 - High Energy Beams: Surface Collision Induced Dissociation

21.5 - Concluding Remarks

Chapter 21 - Reactive Scattering

## 21.1 - INTRODUCTION

Understanding chemical processes at surfaces in general and on metal surfaces in particular is the goal of most heterogeneous catalysis studies. The role of the catalyst in many economically important industrial heterogeneous processes is determined by the details of the interaction of the gas molecule and catalysts' surface. The industrial catalysts typically consist of small metal particles of 10-500 Å in diameter, supported on some high surface area support such as $SiO_2$, $Al_2O_3$ etc. with the aim to obtain a maximum surface to volume ratio of the active metal substance. The overall surface area of those catalysts is measured by hundreds of $m^2$/gr of catalyst. In order to study surface reactions on the molecular level, however, one must look at well characterized and clean surfaces as model catalysts (Somorjai, 1981). These are typically small metal discs with surface area of ca 1 $cm^2$, made of polycrystalline foils or preferably single crystals with known surface orientation and atom arrangement. The knowledge of surface atoms' structure is of great importance in the study of reactions which are surface structure sensitive.

Among the various techniques used for the study of the interaction of gas atoms and molecules with surfaces, the molecular beam-surface scattering experiments are so designed to provide valuable information on the dynamics and kinetics of interactions on a small model catalyst. Three characteristics of these experiments allow the interaction details and intermediate surface reaction steps to be probed. First the collimated flow of reactants of known incident energy provides precise control of reactants' concentration and energy

content on the surface. Secondly, the same features prevent collisions and interactions with surfaces other than the sample to be studied and finally the possibility to square wave modulate or to pulse the reactant gases is essential and unique to this technique in enabling a real time kinetic data collection of such surface processes.

The use of directional and modulated molecular beam in order to deliver reactants to the catalysts' surface was first introduced by Smith and Fite (1963). Their technique was later developed to what is called the modulated beam relaxation spectrometry (MBRS) technique to study heterogeneous kinetic processes by several groups. Several reviews described the type of information which may be obtained by using this technique (Merril, 1970; Jones et al., 1972; Schwartz et al., 1974) along with some of the difficulties which are inherent to it (Olander, 1977). By transforming the originally high vacuum experiment, where the surface cleanliness is not well controlled to an ultra high vacuum (UHV) experiment (West et al., 1971), this method that was carried out on single crystal surfaces of well characterized structure and composition became a very powerful tool in the study of heterogeneous reaction mechanisms on the molecular level.

In this chapter we will describe the important features, the data analysis methods and a few modifications of this important method (MBRS) for the study of surface reaction kinetics and mechanisms. New and different beam sources as well as new detection techniques (using optical methods) for the analysis of the scattered products will be discussed. Electrochemical guns as a source for highly reactive effusive beams that may be modulated at various lineshapes and high kinetic energy supersonic beams as a tool for collision induced chemical reactivity will be described as well.

## 21.2 - METHODS

Molecular beam-surface scattering machines typically consist of two major sections: (i) The molecular beam source which delivers the beam of reactant molecules and (ii) the scattering chamber where the interaction between the reactant molecules and a solid surface - frequently a single crystal sample takes place and where the gas phase species, reactants and products are detected.

In the following we will discuss the experimental requirements pertinent to these two major sections, starting with the scattering chamber, then describing the different types of sources that are used. Most of these experimental details are common to molecular beam studies in general - both in gas phase and in non reactive surface scattering experiments. These subjects are covered in detail in Parts I and II and also in some of the chapters of Part IV of this book, therefore only a brief description will be given here, with emphasis on variations which are important for reactive scattering experiments. Then a description of the type of data analysis which may provide kinetic information on surface reaction will be outlined, mostly regarding the modulated beam relaxation spectrometry (MBRS) technique.

### 21.2.1 - Scattering Chamber

The study of the interaction of gas atoms and molecules with surfaces and in particular those which involve strong interaction that may lead to reactive scattering, require a very low pressure at the scattering chamber. Thus UHV conditions ($P < 10^{-7}$ Pa) are usually necessary to enable an interaction of the gas atoms and molecules with a clean sample for a period of 20 minutes

or longer. These are the typical conditions found in recent reactive and non reactive molecular beam surface scattering experiments (Ceyer et al., 1977; Cardillo, 1981). The preparation and characterization of the samples in these studies, are conducted by common UHV methods, as described in previous chapters. Briefly, when using transition metal single crystals as model catalysts, for example, these are cleaned by several different techniques such as chemical treatment, or noble gas ion sputtering while refractory metals may be kept clean by heating to very high temperatures as well. After a cleanliness test of the samples' surface by means of Auger electron spectroscopy (AES) or ultraviolet or X-ray photoelectron spectroscopies (UPS and XPS) it is annealed to restore the long range order of the surface atoms.

The surface order is probed by means of low energy electron diffraction (LEED) or in the case of molecular beam machines, also by diffracting He beams from the annealed surfaces (Chapter 16) or by monitoring the width of the specular He beam that is back-scattered from the surface.

The detection of the scattered molecules can be accomplished in several ways. The most common of them are techniques which involve the ionization of the gas phase molecules by the interaction with electrons (~70 eV) emitted from a hot filament. These detectors can be of the ionization gauge type, where the total ion current due to a single mass to charge ratio is detected. The first class, when closed in a box with a single aperture is sensitive to the total flux of molecules scattered from the surface and therefore is useful and simple to operate in the non reactive scattering experiments where the incident and scattered atoms or molecules are the same.

The second and more versatile class of detectors are the quadrupole mass spectrometers. The mass selectivity is essential for reactive scattering experiments where the products are unknown and sometimes several different products and some of the reactant molecules may scatter at the same time. In many cases and in particular for low probability catalytic processes there may be severe background problems. In order to improve signal to background ratio at the detector, it is sometimes encapsuled in a differentially pumped chamber inside the UHV scattering section. The detector chamber may even be separated from the main scattering area by an additional "Buffer" chamber, also differentially pumped. An example of such an apparatus was described in detail in ref. 10 and is shown in Fig. 21.1.

The detectors may be either fixed or rotatable about the crystal surface. The fixed detector design is more suitable to reactive scattering studies, where the angular resolution of the scattered molecules should not be very high and most of the information may be obtained by the rotation of the sample about the fixed incident beam. The rotatable detectors are necessary, however, for molecular beam-surface diffraction experiments, where angular resolutions of less than $1^{o}$ are desired. Apparata of this kind were described in the literature for both reactive (Ceyer et al., 1981) and more diffraction oriented (Cardillo et al., 1978; Engel, 1978) machines. An example of such an apparatus which incorporates also time-of-flight measurements capability is shown in Fig. 21.1

A new class of detection techniques were incorporated into the molecular beam surface scattering experiments in the last four years. These are the laser induced fluorescence (LIF) (Frenkel et al., 1981; McClelland et al., 1981;

Kleyn et al., 1981; Cavanagh et al., 1981; Hepburn et al., 1982) and multiphoton ionization techniques (Zacharias et al., 1982; Asscher et al., 1982; Mayden et al., 1982). These optical methods are less widely applicable techniques and generally less sensitive than the quadrupole mass spectrometry. Only six molecules to date (NO,CO,HF,$I_2$,$N_2$ and $H_2$) were shown to be detectable under the low densities typical to these experiments, the NO being the most popular. The importance of these techniques however is in providing information on the internal state distribution of the scattered molecules. This information is essential for better understanding the dynamics of interactions of gas molecules with surfaces.

In the case of reactive scattering, the internal state distribution of the product molecules may help scrutinizing complex surface processes and possibly identify the rate limiting step.

The experimental setup usually consists of UV windows to allow a tunable UV laser beam to intersect with the flux of scattered molecules, and a collection device - either of emitted light (e.g., fl lens inside the UHV chamber and a photomultiplier outside) if LIF is used or an electron multiplier if multiphoton ionization is applied. In fig. 21.2 a schematic presentation of a rotatable optical detector using two photon ionization is shown.

Finally, the electron impact ionization technique was recently utilized in combination with high resolution emission dispersion for the determination of the internal state of scattered $N_2$ molecular beam from iron single crystal (Levkoff et al., 1984).

The detection of scattered molecules' translational energy distribution by means of time-of-flight (TOF) methods as described in chapter 14, is found in only very limited number of reactive scattering experiments. This is due to the experimental difficulty inherent in such measurements. The information that may be obtained, however, together with angular distribution of the scattered species, is of fundamental importance to the understanding of detailed dynamical aspects of the rate limiting step involved in the catalytic surface reaction. Examples of experiments of this kind will be given below.

None of the detection techniques briefly mentioned above are unique for the study of reactive scattering experiments. One modification of the TOF detection techniques which is very important for reactive scattering is the positioning of the chopper for TOF analysis of the scattered products, between the crystal and the quadrupole mass spectrometer. Very often in beam-surface scattering experiments the incident beam is chopped rather than the scattered one and thus the unknown surface residence time of the products may cause error in the kinetic energy determination.

### 21.2.2 - Sources

The various types and configurations of atomic and molecular beam sources are discussed in chapters 2-4. For reactive scattering of molecular beams from surfaces, three source configurations are being used: 1) Effusive source; 2) Multichannel capillary array; 3) Free jet - supersonic source.

Effusion sources are the simplest to make and therefore were the first type of molecular beam sources used in surface scattering experiments (23). It is generally a temperature controlled oven with a small orifice directed

toward the sample. The gas in the oven at pressures less than 1 torr effuses out to the scattering chamber with a Maxwellian energy distribution at the oven's temperature. The angular distribution of the effusing molecules is cos $\theta$, where $\theta$ is the angle from the normal to the orifice. This causes a relatively small flux of reactant molecules at the sample's surface of about $10^{13}$ particles/$cm^2$.sec. This small flux is the major drawback of these sources for surface scattering experiments in general and reactive scattering in particular. Surface reactions with small probability are very difficult to study due to signal to noise problems. When coupled with a UHV scattering chamber, the source chamber is differentially pumped. A chopper is frequently installed in the source chamber or the buffer chamber (a second differentially pumped section before the scattering chamber) to enable time resolved measurements.

There is also a quite different family of sources, that should be considered as effusion sources, and these are the electrochemical guns. These sources generate highly reactive gas molecules such as halogens and sulfur by controlling the electrochemical potential (McKinley, 1964; Spencer et al., 1983), and therefore are used only for reactive scattering studies. The principle of operation depends somewhat on the gas to be evolved from the gun. In the case of the chlorine source, as shown in Fig. 21.3, for example, one sees a pellet of AgCl placed between two electrodes: a silver wire cathode and a pt gauge anode. The connection between the electrodes and the AgCl is achieved by pouring the molten AgCl on top of the spiral silver wire which is the cathode and immediately after the pt gauge is attached to this molten salt. The gun is basically a glass tube which serves both as the

support and as a collimator for the evolved beam. The electrical conductivity is achieved by the electrical field induced motion of $Ag^+$ ion through defects in the AgCl lattice. To facilitate this motion the glass tube is heated to about 420 K, which also determines the "temperature" of the emitted $Cl_2$ molecules. A very convenient advantage of this electrically driven molecular beam source is the ability to generate modulation waveforms of various shapes (Spencer et al., 1983) and thus enable more accurate data analysis as will be discussed below. Unlike ordinary effusive sources here the reactant gas is at a constant temperature, which is the highest possible temperature (to obtain highest flux) such that no sublimation of AgCl occurs. A high degree of collimation is usually not attempted with these sources, since at the high reactivity of the emitted particles, where unity sticking probability is often found, the incident angle of the reactant beam is not important.

The second type of sources are the multichannel capillary array. This is basically an effusive oven fitted with a small opening composed of a large number of very fine capillary tubes. The length to diameter ratio of these tubes is of the order of 50 to one. As a result the beam of molecules effuses out is peaked along the normal to the source opening. In this way higher fluxes are attained at the target for the same leak rate. These sources can usually be operated at pressures somewhat higher than the ordinary effusive sources, which further increases the flux. The energy distribution of the beam is experimentally determined to be nearly Maxwellian, with a slight increase of fast molecules contribution on the expense of the low energy ones. These sources were investigated in detail by Olander and coworkers in a

series of papers in which such sources were utilized for reactive scattering experiments (Olander et al., 1969, 1970a, 1970b).

Finally the free jet supersonic sources are the high intensity, narrow velocity distribution and highly collimated sources, more typical in non reactive molecular beam-surface scattering or diffraction studies. The high intensity of the beam at the target may facilitate enhancing bimolecular surface reactions, thus enabling the study of slower and less efficient catalyzed reactions. In some cases, the large and adjustable translational energy of the beam (0.1-20 eV) (see Chapter 2) is employed to study activated adsorption and dissociative adsorption processes, as will be discussed below. Temporal information may be obtained by using a mechanical chopper in the source or in the second differentially pumped chamber (buffer) if a continuous source is used, or by using a pulsed nozzle source (see Chapter 3).

Reactive scattering studies require more than one reactant molecule in all cases except the simplest surface reaction of dissociation followed by recominative desorption. In most experimental studies one of the reactant molecules is in the background, providing a steady state coverage on the surface, while the second reactant is in the beam. If the beam is chopped, the product temporal behavior can be studied and thus kinetic information on the surface reaction is obtainable. In cases where particularly high surface concentration reactants is desired, for example when inefficient reaction is studied yet low background pressure is necessary, both reactant molecules may be delivered to the sample by two separate free jet supersonic beams. Such an apparatus is shown in Fig. 21.1 and is discussed by Ceyer et al., 1981.

21.2.3 - Data Analysis

It is possible to obtain useful kinetic information on surface reactions and thus to unravel surface reaction mechanism by using the modulated molecular beam technique. In this part, therefore, we will discuss some of the principles behind the data analysis, that may provide such kinetic data.

A beam of molecules impinging on a surface with intensity $I_0$, when mechanically chopped at angular frequency $\omega$, can be thought of as a modulated driving function. When a surface reaction takes place, this modulated function is modified by the chemical processes at the surface. A beam of products leaves the surface with different modulation. By monitoring the waveform of the product beam as a function of incident beam modulation frequency, intensity and energy and as a function of surface temperature, topography and chemical composition, incident beam angle and scattered beam angle - models for the surface reaction mechanism can be formulated and compared with the experimental waveform behavior. In principle the Fourier analysis of the products' waveform should provide the necessary information to come with a reaction mechanism no matter if it is a linear or nonlinear surface reaction. The data analysis in the case of linear processes, however, is far simpler. In a linear system, each Fourier componenet behaves independently of the others. Therefore only the response of the surface to the fundamental frequency component of the modulated incident molecular beam need to be considered. The gating function of the incident beam therefore may be sinusoidal, for example, regardless of the actual waveform:

$$g(t) = g_0 \, \ell^{i\omega t} \qquad [1]$$

where $g_0$ is the amplitude and $\omega$ is the chopping angular frequency.

As an example of the analysis, we shall consider a simple first order process such as the dissociative adsorption of a gas molecule followed by the desorption of an atom A(4):

$$A_2(g) \rightarrow 2A(\underline{ads}) \xrightarrow{k} A(g) \qquad [2]$$

The surface mass balance describing the time variation of the surface concentration of A(ads) ($n_A$) would be:

$$\frac{dn_A}{dt} = 2\,S \cdot I_0 g(t) - k\,n_A \qquad [3]$$

where $I_0$ is the intensity of the incident beam, S is the sticking probability and k is the desorption rate constant. Substituting a trial solution for $n_A(t)$:

$$n_A(t) = n_A^* \ell^{i\omega t} \qquad [4]$$

and the gating function in eq. [1] into eq. [3] gives:

$$i\omega n_A^* \ell^{i\omega t} = 2\,SI\,g_0 \ell^{i\omega t}_0 - kn_A^* \ell^{i\omega t}$$

The steady state solution for $n_A^*$ gives:

$$n_A^* = \frac{2\,SI_0 g_0}{k+i\omega} \qquad [5]$$

$$kn_A^* = \frac{2\,SI_0g_0e^{-i\tan(\omega/k)}}{[1+(\omega/k)^2]^{1/2}} \qquad [6]$$

A reaction product vector can be defined ($\bar{\varepsilon}$) which is the ratio of scattered product signal to incident reactant flux. In the limit of low reaction probabilities this vector is given by the ratio of $kn_A^*$ to $I_0g_0$, modified by a phase factor, which is related to the surface residence time of the products:

$$\bar{\varepsilon} = \left[\frac{k\,n_A^*}{I_0g_0}\right] e^{i\phi} = \varepsilon e^{-i\phi} \qquad [7]$$

Equation [6] can then be rewritten as:

$$\varepsilon \cdot e^{-i\phi} = \frac{2S^{-i\tan(\omega/k)}}{[1+(\omega/k)^2]^{1/2}} \qquad [8]$$

Therefore $\varepsilon$, the ratio of products to reactants fluxes is given by:

$$\varepsilon = \frac{2S}{[1+(\omega/k)^2]^{1/2}} \qquad [9]$$

and $\phi$ the phase difference between product and reactant signals is given by:

$$\phi = \tan^{-1}(\omega/k) \qquad [10]$$

By observing the amplitude and phase of the product and reactant signals as a function of chopping frequency $\omega$, k the desorption rate constant can be determined by a plot of tan $\phi$ vs. $\omega$. The sticking probability S may be determined by a plot of $1/\varepsilon^2$ vs. $\omega^2$. The values of $k(T_s)$ at several surface

temperatures ($T_s$), can give the kinetic parameters of the desorption process - activation energy and preexponential factor for an Arrhenius type rate constant.

Practical complications in the detection of the desorbed A(g) species may arise in cases where the sticking probability is less than unity. In such cases some of the reflected $A_2$(g) molecules may contribute to the signal of A(g) and thus make the exact measurement of A(g) more difficult to obtain. There are, however, differences in the angular and velocity distributions of the reflected compared with the trapped-desorbed atoms. The reflected molecules are typically scattered in a lobular angular distribution centered near the specular angle ($\theta_{scattered} = \theta_{incident}$) while the trapped desorbed molecules will be scattered in some cases at a cosine angular distribution or in other cases with a distribution which is peaked at the normal to the surface. The velocity distribution of the reflected molecules typically depends on that of the incident beam and the surface temperature (Hurst et al., 1979; Janda et al., 1983), while this of the desorbed atoms is characteristic of the surface temperature and the surface reaction involved and is independent of the incident beam energy. These differences in the typical behavior of these two phenomena can help separating between them and pick up the desired signal.

For first order processes such as that discussed above, in cases where one may assume that both S and the angular distribution of the desorbed particles are independent of the surface temperature, the values of $k(T_s)$ may be obtained by measuring only the signal amplitude at a given surface temperature divided by that obtained at high surface temperature (where $k(T_s) >> \omega$). The

only difficulty in this procedure is the higher sensitivity of amplitude measurements to the velocity distribution of the measured species, and thus the conversion from density to flux distributions may contain errors if an unknown deviation from a complete accommodation of the desorbed species with the surface occurs (D'Evelyn et al., 1983). The origin of this difficulty is that the mass spectrometer's signal, which is proportional to the density of particles, will be inversely proportional to their speed at any given flux.

At modulation frequencies where the phase angle is changing appreciably with $T_s$, $k(T_s) \sim \omega$ and the surface coverage may be estimated as:

$$n_A^* = \frac{I_0 \cdot S}{k} \cong \frac{I_0 \cdot S}{\omega} \qquad [11]$$

This expression tells us that under typical MBRS experimental conditions such as an incident reactant flux of one monlayer per second, a sticking probability of one and modulation frequencies of 100-1000 Hz, the surface coverage $n_A^*$, during the experiment should be of the order of $10^{-2}$-$10^{-4}$ of a monolayer. Therefore the $k(T_s)$ values obtained in MBRS experiments are those corresponding to low surface coverage.

The analysis shown above for the simple adsorption-desorption process may be extended easily to a sequential or parallel first order processes as was shown by Jones et al. (1982). For the linear sequential process below:

$$A_2(g) \xrightarrow{n} 2\,A_{ad} \qquad [12]$$

$$A_{ad} \xrightarrow{k_1} B_{ad}$$

$$B_{ad} \xrightarrow{k_2} B(g)$$

the reaction product vector ($\bar{\varepsilon}$), sometimes called also the surface transfer function, is shown to be (4):

$$\bar{\varepsilon} = \frac{2S}{[1+(\omega/k_1)^2] \cdot [1+(\omega/k_2)^2]} e^{i\phi} \qquad [13]$$

where

$$\phi = \tan^{-1}(\omega/k_1) + \tan^{-1}(\omega/k_2) \qquad [14]$$

Equations [13] and [14] show that for a sequence of linear processes, the phase lags of each step are additive and the amplitude factors are multiplicative.

This type of analysis was further developed for branch processes and diffusion limited surface processes as well, Jones et al. (1972).

A polar plot of $\bar{\varepsilon}$ provides a convenient means of determining the significance of processes in the surface reaction mechanism that involve more than a single step. Such polar plots are shown in Fig. 21.4 for (a) adsorption-desorption; (b) a two-step sequence with $k_1 = k_2 = k$ and (c) a parallel branched reaction process with a branching probability of 0.5 (32). A different way to analyze linear reaction mechanisms that can treat more complicated linear schemes was suggested by Chang and Weinberg (1977a, 1977b) who formulated a matrix notation for the kinetic equations with the concentrations of the various surface intermediates as the matrix elements.

To conclude this section on the analysis of linear surface processes the Fourier analysis of products' waveform should be mentioned. This method was applied to linear systems by Foxon et al. (1974) and others and then was

extended by Sawin et al. (1981) who showed the significance of high harmonics of the scattered products waveform (as high as 29th) to the understanding of the reaction mechanism, by using a square wave incident beam (which includes only odd harmonics). It was shown to compare favorably with the lock-in detection technique mentioned above and other techniques such as the cross-correlation modulation and pulse testing, Sawin et al. (1981).

Finally, a few words on nonlinear surface reactions. The analysis of these is far more complicated than the linear processes. In nonlinear reactive scattering systems one includes those processes for which the kinetic equations contain the product of two or more time varying quantities. Examples for nonlinear surface kinetics are second order desorption (desorption following adatom recombination) with a coverage dependent sticking probability. A nonlinear process is indicated experimentally by a phase lag that is very sensitive to the incident reactant beam flux (D'Evelyn et al., 1983). Also the detection of harmonics in the products' waveform Fourier analysis that do not appear in the incident beam (e.g., even harmonics with square wave incident beam modulation).

The kinetics of a nonlinear surface process may in principle be determined by numerically integrating the kinetic equations, combined with a Fourier analysis of the products' waveform (Foxon et al., 1974). Alternatively, a method of linearization was suggested by Schwarz and Madix (1974), in which the experimental conditions are modified such that the kinetic equations become linear. This technique requires a fairly high flux of one of the reactants, so that the modulated beam represents a small perturbation on the total flux on the surface (Schwartz et al., 1974). In this case, only the

fundamental harmonics of the modulated products flux should be considered (Olander et al., 1976). More on nonlinear surface processes can be found in D'Evelyn et al. (1983).

It should be stressed, that there is a considerable ambiguity in the assignment of reaction mechanism to the analyzed data as it was presented here, mostly for more complicated surface reaction mechanisms. This problem, with the advantages and weaknesses of the MBRS technique were discussed in detail by Olander (1977).

The interpretation of surface catalyzed reactions is based on two widely accepted classes of surface reaction mechanisms. The first is the Langmuir-Hinshelwood where the rate limiting step involved the reaction between species in the adsorbed state. This mechanism is probably the most general and common among heterogeneously catalyzed processes. In terms of reactive scattering experiments the observation of a phase lag of any kind in the flux of products compared to the incident reactants' waveform as will be discussed in the next section of this chapter, ensures the dominance of this mechanism. The second called the Eley-Rideal mechanism, involves in its rate determining step, the direct reaction between a gas phase reactant and an adsorbed surface species. Such a mechanism should not show phase lag in any reaction conditions. While a possible mechanism in realistic high pressure industrial processes, it was never shown unambiguously in a well controlled, reactive scattering experiment to exist.

## 21.3 - REACTIVE SCATTERING: EFFUSIVE BEAM SOURCES

The introduction of the modulated molecular beam technique for the first

time by Smith and Fite (1963) involved an apparatus which contained an effusive continuous source of rare gas atoms. The atomic beam was then chopped inside the scattering chamber and the angular distribution of He atoms scattered from a freshly evaporated thin film of gold was measured. The same technique was later applied to scattering studies of Ar and He from evaporated films of silver and gold as well (Smith et al., 1964). In both studies angular distributions that are peaked near the specular angle were found when the surface could be considered flat and clean. The base pressure in those studies was relatively poor, about $8.10^{-7}$ torr.

21.3.1 - $H_2$-$D_2$ Exchange and Recombination Reactions:

By employing effusive beams from an oven source at temperatures up to 2700 K, the same authors (Palmer et al., 1970) could study the reactive scattering of HD, following deuterium-hydrogen exchange reaction. This reaction may be considered the simplest of all reactive scattering systems. It was studied on a Ni(111) film epitaxially grown on a mica substrate. Having a beam of $D_2$ and an ambient of $H_2$ molecules or vice versa, they followed the HD exchange product as a function of various experimental parameters (Palmer et al., 1970). It was found that the angular distribution of the desorbed HD molecule varied as $\cos^d\theta$ with $2.5 < d < 4.0$, where $\theta$ is the reflected angle with respect to the surface normal. The value of d was found to be sensitive to the conditions of the surface such as smoothness and cleanliness: The more smooth and clean is the surface, the higher d is. They also found an increase in the yield of HD produced on the Ni(111) film when the beam energy was raised to 1800 K from room temperature. This observation implied the

existence of an activation energy for adsorption of about 2 kcal/mole.

The details of the hydrogen deuterium exchange reaction attracted further studies using molecular beam techniques. Under UHV conditions, using well defined single crystal surfaces, Bernasek et al. (1973, 1975) had shown that the yield of the HD production is higher on high Miller index stepped surfaces such as the (997) face than on the flat (111) face.

The HD production yield increased with the density of ordered arrays of one atom high steps, as was shown by the enhanced reactivity of the (553) face compared with the (997) high Miller index plane (Bernasek et al., 1975). The (553) face had almost twice the steps density of the (997) surface. In Fig. 21.5 the signal intensity of $H_2$, $D_2$ and the exchange product HD are given as a function of the scattering angle measured from the surface normal on the three platinum single crystal surfaces, (111), (997), and the (553).

The exact role of steps in enhancing this exchange reaction was then studied by using the unique feature of a molecular beam - its directionality. In a series of papers, Gale et al. (1977) and Salmeron et al. (1977, 1979) had shown that a marked increase in the production of HD is obtained if the beam of reactants strikes the open side of the steps (Gale et al., 1977). This effect was demonstrated by varying both the angle of incident beam with respect to the surface normal ($\theta$) and the azimuthal angle ($\phi$). In Fig. 21.6 the effect of varying the incident angle ($\theta$) at a fixed azimuth ($\phi = +90^{o}$) on the HD production rate on a pt(332) single crystal surface is shown. The effect of the azimuth at a fixed angle of incidence is shown in Fig. 21.7.

It was concluded that the activity for H-H bond breaking at a step site, equals about seven times that of a terrace site at normal incidence (Salmeron

et al., 1977). The observations further implied that the inner corner of the step structure is the most active site for the dissociaiton of hydrogen molecules. All the studies (described by Bernasek et al., 1973, 1975; Gale et al., 1977; and Salmeron et al., 1977, 1979) employed a relatively intense and better directed effusive molecular beam source by using a multichannel capillary array. This source could also be heated for providing a translationally hot molecular beam. This capability is particularly convenient for the determination of an activation energy for adsorption (Bernasek et al., 1975) and will be described further in chapter 21.4.

The same $H_2$,$D_2$ exchange reaction was studied extensively also in order to determine the hydrogen adatom recombination kinetics. Using molecular beam relaxation spectrometry techniques, several groups have measured the activation energy and preexponential factors for this recombination reaction. Using the measured phase lag and signal intensity according to the equations in chapter 21.2, those parameters could be obtained. As was pointed out by Olander (6), however, the values obtained are very sensitive to the kinetic model adopted. Therefore, it is not surprising to find in the literature large discrepancies in the kinetic parameters reported after employing different methods and even between different groups, who used the same technique, but assumed different kinetic models. Such is the case for example, if the values reported by Christmann et al., (1976) and Salmeron et al., (1979) are compared, both employed the MBRS technique. The former found a preexponential parameter of $10^{-2}$ $cm^2 \cdot sec^{-1}$ and an activation energy of 16 kcal/mole for the same reaction of hydrocarbon deuterium recombination on top of a pt(111) single crystal surface. Different kinetic parameters were

obtained by employing other techniques, as summarized in D'Evelyn et al., 1983.

Applying the MBRS method with a multichannel array neutral beam source capable of delivering a chopped beam of about $10^{14}$ particles/$cm^2$ sec, Gdowski, Fair and Madix (1983) have shown $D_2CO$ and $CH_3OD$ to decompose rapidly on pt(110) and on the stepped Pt(s)-[9(111)x(100)] surfaces. The rates measured for the evolution of CO following $D_2CO$ or $CH_3OD$ decomposition were identical to those reported previously for the desorption of CO from the same surfaces (Fair et al., 1980; Gdowski et al., 1982), indicating a desorption limited sequence of elementary steps. The rate measured for the hydrogen evolution on pt(110) was given by $10^{0.0\pm0.5}$ exp[-24 kcal/mole/RTs] $cm^2$ $sec^{-1}$, while on the stepped surface the MBRS data were analyzed as a branched process (Gdowski et al., 1983). Further analysis of this branched reaction in the presence of background CO molecules or a surface-poison of 10% sulfur atoms, which block preferentially the steps, have indicated that the fast branch occurs at terrace sites, while the slower one on steps sites (Gdowski et al., 1983). See Fig. 21.8.

21.3.2 - CO oxidation

Oxidation of CO on metals is another example of a surface reaction of great interest that was extensively studied. Several interesting features of this reaction were addressed such as the oscillations of the $CO_2$ production rate at relatively high reactants pressures and on ill-defined metal surfaces (Turner et al., 1982). This phenomenon was studied under well defined conditions and on single crystal surfaces by Ertl et al. (1982), Cox et al.

(1983) and by Yeates et al. (1985). The dynamics and energy disposal following this highly exothermic surface reaction were studied as well, mostly by employing supersonic molecular beam techniques, as will be briefly described in Chapter 21.4. The use of MBRS methods, however, was of great importance in scrutinizing the basic questions about the mechanism of this reaction.

Earlier studies of the CO oxidation could not distinguish between two possible reaction mechanisms:

a. Eley-Rideal (ER) mechanism in which a reaction occurs directly between an adsorbed oxygen atom and an incident gas phase or physisorbed CO molecules. In such a mechanism the product $CO_2$, which is only weakly bound to the metal surface, is emitted instantaneously to the gas phase. This was suggested as the reaction mechanism by Pacia et al. (1976) and Winterbottom (1973).

b. Langmuir-Hinshelwood (LH) mechanism describes the reaction between adsorbed oxygen atoms and adsorbed CO molecules. Here the reaction product yield should be sensitive to surface parameters such as reactants' coverage, surface temperature and relative $CO/O_2$ flux at the surface. The dominance of the LH mechanism was clearly demonstrated by Engel and Ertl on pd(111) (Engel et al., 1978) and by Campbell et al., 1980 on a pt(111) surface, by following the phase lag and temperature dependence of the $CO_2$ product after modulating either the CO or the $O_2$ incident beams with the other reactant as an ambient background. Similar results were found by Fair and Madix (1980) who studied this reaction on a stepped pt[9(111)x(100)] surface and earlier by Palmer and Smith on a pt(111) film (1974). The kinetic parameters determined revealed a strong dependence of the reaction rate on the surface coverage

(Engel et al., 1978; Campbell et al., 1980). The coverage dependence of the CO oxidation rate, was attributed to oxygen adatoms islands formation at high coverages due to attractive interactions (Conrad et al., 1978). This was implied by the inhibition of oxygen adsorption at the presence of previously adsorbed CO, while relatively large oxygen coverage did not change much the initial sticking probability of CO (Conrad et al., 1978; Gland et al., 1983). The second order rates measured for the $CO_2$ production were $10^{-5.4}$ exp(-12 kcal/mole) $cm^2$ $sec^{-1}$ and $10^{-7}$ exp(-10 kcal/mole) $cm^2$ $sec^{-1}$ (Fair et al., 1980) for the reaction on pt(111) and the stepped pt[9(111)x(100)] surfaced respectively, both at saturation oxygen coverage and very small CO coverage.

More details on this surface oxidation reaction were written in a recent review by Engel and Ertl (1982).

Several more complicated surface reactions were studied as well, the kinetic parameters and reaction mechanisms of which were determined by MBRS techniques by employing effusive beams. Among those systems are the deuterium oxidation on pt(111) (Smith, Jr., 1972) to form deuterated water, the interaction of oxygen (Olander et al., 1972; Jones et al., 1972) hydrogen (Balooch et al., 1975) and water (Olander et al., 1977) with a pyrolitic graphite surface and the ammonia decomposition on the flat (111) and stepped platinum surfaces (Guthrie et al., 1981) to mention just a few of them. Reactions on semiconductors were studied as well (Farnaan et al., 1984). As pointed out by Olander (1977), the reaction mechanisms may involve many steps, particularly in more complicated surface processes, and then the MBRS analysis schemes of Chapter 21.2 rely heavily on the assumed reaction mechanism. In

such cases, the kinetic parameters obtained may be sometimes ambiguous.

21.3.3 - Highly reactive beams

The surface reactions of reactive gases such as halogens and sulfur, are not simple to study in a clean UHV environment. Those gases tend to stick to the UHV chamber and to stay as a background for a long time. Yet several studies employing halogens from effusion sources or using novel solid state electrochemical sources were published. Some of these studies are described below. A molecular fluorine beam from a quartz multichannel array effusion source, was employed by Machiels et al. (1977a,b) who study the kinetics of the interaction of $F_2$ with polycrystalline tantalum (Ta) and with uranium dioxide. In both studies the molecular beam relaxation spectrometry (MBRS) technique was employed for the determination of the kinetic parameters of the complicated surface reaction. In the study of the reaction of $F_2$ with Ta, the sole volatile product at surface temperatures of 690 to 930 K was $TaF_5$. A surface reaction mechanism involving a thin scale of $TaF_3$ on the surface, and diffusion of adsorbed F atoms through this scale as a step which governs the reaction rate, was suggested Machiels et al. (1977a,b).

At higher temperatures, the reaction of $F_2$ with $UO_2$ (Machiels et al., 1977a) was shown to produce only $UF_4$ at surface temperatures above 1000 K. Here again surface diffusion and diffusion to the bulk are important ingredients of the reaction mechanism. Some indirect indication for the presence of atomic fluorine was noted at the higher surface temperatures. While these two systems are quite normal in terms of the effusive sources at high vacuum environment, in subsequent studies by the same group, chlorine

beams were scattered from molten metal surfaces - an unusual application of the MBRS technique. The reaction of $Cl_2$ with solid and molten indium surfaces was studied (Balooch et al., 1984a) at surface temperatures of 300-650 K, and also with molten lead surfaces (Balooch et al., 1984b). While in the first system $InCl_2$ is formed predominantly at low surface temperatures, at higher temperatures, where the interaction of $Cl_2$ is with the liquid phase, InCl is the only observable product (Balooch et al., 1984a). A drastic change of the sticking probability of $Cl_2$ at the melting point indicates the possible change from a clean indium surface at high temperatures to a chlorine covered one at low temperatures. This is consistent with a decrease of the reflected $Cl_2$ molecules by an amount which is similar to the overall reaction probability which occurs near the melting point.

The only product found by scattering $Cl_2$ from lead is $PbCl_2$, over the entire temperature range of 300-400 K. The reaction probability increased rapidly near the melting point, changing non linearly with the temperature, as can be sseen in Fig. 21.9. The mechanism of this reaction is suggested to involve parallel Eley-Rideal and Langmuir-Hinshelwood mechanisms (Balooch et al., 1984b)

The studies mentioned above utilized a multchannel capillary array to generate the effusive beams, therefore could obtain a relatively high flux of halogen molecules impinging on the target's surface. The beam was mechanically chopped at frequencies of 2-1000 Hz. These studies, however, are done at high vacuum conditions ($\sim 10^{-6}$ Pa) therefore the cleanliness of the surface is difficult to maintain.

A different approach to the delivery of a beam of halogen molecules in a

clean UHV environment was presented by Spencer et al. (1980,1983). These authors employed a solid state electrolysis concept, as described in section 21.2, in order to control the flux intensity, and the temporal behavior of the halogen cell. By measuring the current through the electrochemical cell, they could stechiometrically "count" the intensity of the chlorine molecules evolving from the Ag/AgCl/Pt cell, the Ag and Pt ends being the cathode and anode respectively . The electric field between the electrodes induced the motion of $Ag^+$ ions through defects in the AgCl lattice. The evaporation of $Cl_2$ at the anode side of the chlorine gun could therefore be controlled by applying any desired voltage waveforms between the electrodes. This could be done, for example, by remote control of a microcomputer, which by an appropriate programming could deliver the wanted waveforms. In Fig. 21.10 an example of a few of those synthesized potential waveforms and the corresponding $Cl_2$ emission waveforms is shown. The different waveforms typically contained several odd harmonics at equal amplitude as a tool for reaction mechanism determination (Spencer, 1980).

Two features of this electrochemical gun make reactive molecular beam surface scattering experiments difficult to perform. The relatively low flux of reactants at the surface, the maximum of which was measured to be a $5 \bullet 10^{13}$ molec/$cm^2 \bullet$sec and the poor colimation (Spencer 1980). The low beam intensity caused severe signal to nois problems in the AgCl products' waveforms analysis. Such chlorine gun was employed for the study of the interaction of $Cl_2$ with Ag(111) under UHV conditions. By monitoring the AgCl (142 a.m.u.) and Cl (35.5 a.m.u.) in a thermal desorption experiment following a saturation coverage dosage of $Cl_2$ on the Ag(111), these authors concluded

that AgCl is the major desorbing species. Despite signal to noise problems the authors could identify odd harmonics to dominate the AgCl products' waveform frequency domain. No exact kinetic parameters for the AgCl formation mechanism could be obtained, but thermal desorption studies and the similarity of the results to those obtained previously on the (100) (Kitson et al., 1980) and the (111) (Goddard et al., 1977) faces of silver indicated the presence of adsorbed clorine atoms overlayer on the surface. The presence of a zero order desorption peak in the thermal desorption of AgCl, implied the existence of islands of AgCl on the Ag(111) surface. Arrhenius plots yielded activation barriers for the desorption of AgCl of 96±5 kj/mole (Spencer, 1980), which is much lower than $\Delta H$ for sublimation of AgCl (244 kj/mole).

Similar electrochemical guns were shown previously to deliver bromine (Bertl et al., 1979) and in a somewhat different construction, the electrolysis of $Ag_2S$ in a cell of the $Ag/AgI/Ag_2S/Pt$ form, was successfully used to deliver $S_2$ molecules (Schwaha et al., 1979). The $S_2$ gun was then utilized to study the surface chemistry of $S_2$ on Ag(111).

## 21.4 - REACTIVE SCATTERING: SUPERSONIC BEAMS

Two major advantages of supersonic molecular beams over effusive sources make them particularly useful for reactive scattering experiments. The first is the possibility to obtain high kinetic energies combined with narrow velocity distribution. This feature of supersonic beams was used to study activated dissociative adsorption systems as will be discussed in section 21.4.1. At very high kinetic energies collision induced dissociation phenomenon was reported and will be described in section 21.4.3. The second

advantage of supersonic beams is the high flux of particles at the surface. This advantage is of great importance for the study of slower and less probable surface catalyzed reactions. The high reactants' flux generate also high flux of product molecules desorbing from the surface, thus enables translational energy and internal state distribution determination as a function of the scattering angle and surface temperature. Such information is of great value for understanding the dynamics of the surface reactions. This aspect will be discussed in chapter 21.4.2.

### 21.4.1 - ACTIVATED DISSOCIATIVE ADSORPTION AND ASSOCIATIVE DESORPTION

The possible barrier for adsorption was already mentioned in the previous chapter in the study of $H_2$-$D_2$ exchange reaction on various metal surfaces, using heated effusive sources. The major disadvantage of effusive sources for such an application is the increasing kinetic energy spread of the incident molecules with the source temperature, thus making an accurate determination of the barrier height difficult to obtain.

In the study of the interaction of $H_2$ with various copper single crystal faces, Balooch, Cardillo, Miller and Stickney (1974) had shown that the probability for dissociative sticking of $H_2$ and then the $H_2$-$D_{ad}$ exchange reaction, increased with the normal component of the incident translational energy. This probability on Cu(100), Cu(110) and Cu(310) increased fourfold to about 0.1, by increasing the vertical beam energy component by that amount (from ca ~2 kcal/mole to 8 kcal/mole, where $E_\perp = E_i \cos^2\theta_i$), Balooch et al. (1974). These results had implied the existence of an activation energy for adsorption. In subsequent classical trajectories of these results made by

Gelb and Cardillo (1978) the barrier was determined to be at least 33 KJ/mole. In those studies, Balooch et al. (1974), a single supersonic beam of $H_2$ striked the clean copper surfaces, or surfaces that were preadsorbed with D atoms, in order to follow the exchange reaction. They also determined the angular distribution of the HD product and had reported an excellent agreement with permeation experiments made previously.

In a recent study by Lin and Somorjai (1983, 1984) a different approach was taken in order to study the dynamics of the $H_2$-$D_2$ exchange reaction. They measured the kinetic energy in the HD product on a stepped pt(557) surface as a function of the scattering angle and surface temperature. In their study, two separate supersonic molecular beams were employed (one of $H_2$, the other of $D_2$) and were intersected in a spot of 1.5 mm diameter on the pt sample. The details of their apparatus were gien previously (Ceyer et al. 1981 and Lin et al. 1983).

They have found that the HD molecules desorb at a Maxwellian kinetic energy distribution, at temperatures (defined as the average kinetic energy divided by 2k, where k is Boltzmann's constant) colder than the substrate temperatures at all desorption angles. The average kinetic energy of the scattered HD molecules decreases as the scattering angle increases. These results were different from time-of-flight measurements made by Comsa, David and Schumacher (1980) and Comsa and David (1982) following the recombination of incident $H_2$ beam with permeated D atoms on several metal surfaces. The absence of subsurface D atoms in Lin's experiment (Lin et al., 1984) are thought to be a possible source for the different results. In the experiments by Comsa et al. 1980 and 1982, peaked angular distributions of the scattered

HD were found and were typically associated with a time-of-flight distribution at Maxwellian temperature hotter than the substrates', at a scattering angle normal to the surface. The "hotter" molecules at scattering angles near the normal to the surface are thought to be associated with a barrier for adsorption (Comsa et al. 1982). In order to explain their "Cold" molecules, a precursor model was suggested by Lin and Somorjai (1984) without a net barrier for adsorption (the difference in activation energy for chemisorption and desorption from this precursor state - is negative). This model, however, does not explain the observed surface temperature dependence of the scattered HD mean kinetic energy which is at a roughly constant value lower than the surface temperature between 500-1100 K.

Inertness of gas molecules at surfaces (low sticking probability) may sometimes be associated with a barrier for adsorption. The interaction of $N_2$ molecules with some metals is an example.

The dissociative adsorption of $N_2$ molecules was recently studied by Auerbach, Pfnur, Rettner, Schlaegel, Lee and Madix (1984) and Lee et al. (1984) on the W(110) single crystal face. The sensitivity of this dissociative adsorption to the tungsten surface structure was noted by the experimental observation that room temperature $N_2$ molecules have an initial sticking probability of $S_0 = 0.6$ on the W(100) face, Auerbach et al. (1984) while only $S_0 = 10^{-3}$ on the more closed packed W(110) surface. Using supersonic molecular beam source, Auerbach et al. (1984) have studied the possible existence of a barrier for $N_2$ adsorption on the W(110) as the cause for the low sticking probability. These authors have found that by varying the kinetic energy of the incident $N_2$ molecules between 8 to 210 KJ/mole (by heating the nozzle up to 1000 K and by seeding the $N_2$ in He or $H_2$) the initial

sticking probability rose from $3 \bullet 10^{-3}$ to 0.4. They concluded that the barrier should be about 84 KJ/mole. Fig. 21.11 presents this initial sticking probability increase as a function of incident beam energy at different incident angles. It was found that unlike the $H_2$/Cu system, the initial sticking probability was relatively insensitive to the beam angle of incidence. The saturation coverage was found to be beam energy dependent. It was also shown in this study that the activation energy for adsorption is most effectively surmounted by translational energy as opposed to internal energy. This was indirectly implied by heating an effusive source to 2000 K, where the internal states are having the oven temperature, unlike the nozzle source, and observing a sticking probability that scaled well within the experimental error, with that of a supersonic beam at translational energy equivalent to 2000 K. The contribution for the sticking probability from internally hot molecules is thus negligible (Auerbach et al., 1984).

The reversed reaction, namely the recombinative desorption of $N_2$ from the W(110) surface is expected to show considerable translational and internal energy in the scattered $N_2$ molecules. Such an experiment has not been done yet, but should be of great interest. The results published by Thorman and Bernasek (1981), who reported vibrational energy excitation in $N_2$ molecules following recombinative desorption from sulfur covered iron surfaces, support this expectation. It should be noted however that the barrier for adsorption on iron surfaces was shown to be much smaller than that on the W(110) face (only 21 KJ/mole on Fe(100) (Bozso et al., 1977), therefore energy release into the $N_2$ molecules desorbing from W(110) should be considerably larger than from iron.

Following the reversed reaction, namely the activated recombinative desorption, may provide a different aspect of this subject. The CO oxidation is an example. The use of supersonic molecular beams and the higher flux of products that resulted from it enabled the study of the translation, (Becker et al., 1977) and internal energy (Mantell et al. 1981 and 1983) release into the $CO_2$ products following the CO oxidation on pt surfaces. As mentioned above, the combination of large exothermicity and relatively weak interaction between the $CO_2$ product and the pt surface, cause large portion of this energy to be carried by the desorbing molecules. Becker et al. (1977) had measured the velocity distribution of scattered $CO_2$ molecules following the oxidation for CO on a polycrystalline pt foil and found translationally hot $CO_2$ molecules with an average kinetic energy of $E_K/k$ = 3560 K and $E_K/k$ = 2140 K with detector at the normal to the surface and at $45^o$ from the normal, respectively. They measured also angular distribution of the $CO_2$ molecules and found a peaked distribution varying as $\cos^n\theta$ with n = 2-3, a number which is less than half of the value reported for pt(111) (Palmer et al., 1984). A barrier for adsorption of va. 30 KJ/mole that was predicted by Palmer et al. 1974 was consistent with the translational energy found at the normal to the surface.

The internal energy of $CO_2$ molecules produced by the CO oxidation reaction on a polycrystalline pt foil was extensively studied by Mantell et al. 1981 and 1983, using a very high flux, pulsed CO beam in an ambient oxygen or with two beams which consisted of a continuous oxygen beam and the pulsed CO beam, for temporal resolution of the reaction. They have utilized an FTIR apparatus with a spectral resolution of 0.06 $cm^{-1}$ in order to follow the IR emission of

the desorbing $CO_2$ molecules. They have found an extensive vibrational excitation in the asymmetric stretch mode, about twice the surface temperature. The rotational excitation on the other hand, was found to be composed of two different distributions characterized by two temperatures: one was considerably colder than the surface temperature and was thought to be due to collisionally induced rotational relaxation in the gas phase and the other was hotter than the surface temperature and therefore is believed to contain some of the reaction exothermicity.

All these results and others by Segner et al. (1984) who studied coverage and surface temperature effects on the angular distribution of the $CO_2$ product had led to the conclusion of a substantial barrier for adsorption of the $CO_2$ on pt surfaces. A possible one dimensional potential energy illustration for this system is shown in fig. 21.12.

The reactive scattering experiments described above display some of the various methods that were applied to the study of relatively simple surface reactions.

In the next section of chapter 21.4, two of the more complicated reactions will be described, again using different methods in order to address aspects of the dynamics behind catalyzed surface reactions. These are the deuterium and the ammonia oxidation reactions, both on the flat pt(111) surface.

### 21.4.2 - COMPLEX SURFACE REACTIONS: PRODUCTS ENERGY DISTRIBUTION

The high flux of reactants enables one to measure energy content of products as a function of scattering angle and at given vibrational/rotational states. This advantage was demonstrated in section 21.4.1 for relatively

simple surface reactions and will be described here for the slow catalytic oxidation of $D_2$ to $D_2O$ on pt(111) by following the products' velocity distribution by means of mass spectrometry time of flight analysis (Ceyer, Guthrie, Lin and Somorjai, 1983) and the laser induced two photon ionization of the NO product following ammonia oxidation on the same surface (Asscher, Guthrie, Lin and Somorjai, 1984).

Oxidation of Deuterium:

The experimental set-up for this study was described before by Ceyer et al. (1981). Two separate supersonic beams with the two reactants, $D_2$ and $O_2$, were intersected at the surface. The flux of scattered $D_2O$ products was time of flight (TOF) analyzed by means of a cross-correlation chopper technique. The chopper was placed between the sample and the two stage differentially pumped quadrupole mass-spectrometer, in order to eliminate unknown residence time problems from interfering with the TOF analysis. Angular distributions were measured and thus, the TOF data could be taken as a function of scattered angles as well. In spite of the relatively high flux of reactants, this surface reaction was found to be quite slow, with a typical signal to background count rate ratio of 30-80 to 7000 at m/e = 20, at surface temperatures between 650-913 K.

The angular distribution of the scattered $D_2O$ molecules was found to be isotropic, varying as cos $\theta_f$, as was found earlier by Smith and Palmer (1972). Unlike what might have been expected from an isotropic angular distribution, however, a complete equilibration of the translational energy with the surface was not found. The mean kinetic energy of the $D_2O$ products

was colder than the expected translational temperature if the molecules were Maxwell-Boltzmann distributed at the surface temperature (Ceyer et al., 1983). Time of flight distributions transformed to energy distributions are shown in fig. 21.13. It was found that the mean kinetic energies given in temperatures as $\langle E_k \rangle / 2k_\beta$ varied between 220 to 400 K for surface temperatures in the range of 440-913 K.

These observations were suggested to originate from a non equilibrated desorption of the $D_2O$ product from the pt(111) surface. Such a non equilibrium mechanism was calculated and predicted by Tully (1981) to be important in the desorption of Ar and Xe from pt(111). This mechanism assumes the preferential desorption of molecules in the chemisorption well that had been thermally excited to higher energy levels in the well. This is the case if the thermal excitation is slower than the desorption rate and the result is a distribution on the surface which is depleted of its high energy tail. This colder distribution results in a slower observed velocity distribution of the desorbing $D_2O$ molecules.

The deuterium oxidation reaction to form $D_2O$ on pt(111) is an interesting example to show how much the details of the surface reaction mechanism is important in determining the products energy content. Although the gas phase reaction:

$$D_2(g) + O_2(g) \rightarrow D_2O(g) + O_{ad}$$

is highly exothermic (347 KJ/mole), the details of the surface reaction mechanism indicate that the $D_2O$ is apparently adsorbed to the surface prior to

desorption, and only this way such a cold translational energy distribution is possible.

Ammonia Oxidation

The reaction between $NH_3$ and $O_2$ on commercial pt catalysts proceeds with an efficiency of more than 95% to product NO and $H_2O$. This high efficiency and the exothermicity of the reaction made this reaction a good candidate for the determination of the NO's internal state and angular distributions, following the reactive scattering of $NH_3$ and $O_2$ beams to form the NO products. Such determination was thought to provide the information necessary for understanding the detailed surface reaction mechanism (Asscher et al., 1984).

The apparatus used for this study was identical to the one mentioned before in the deuterium oxidation reaction (Ceyer et al. 1981 and Ceyer et al., 1983), except that the detector was an optical one and that the $NH_3$ beam was mechanically chopped at 10 Hz while the $O_2$ beam was continuous. As described in section 21.2 the optical detection of the NO product utilized a resonant two photon ionization process using a tunable UV laser, Asscher et al., (1982, 1983, 1984). A schematic representation of the apparatus is shown in fig. 21.2. A time synchronization between the mechanical chopper and the laser trigger via a continuously variable delay enabled Asscher et al. (1984) to follow the evolution of the NO production rate in real time as a function of the surface temperature and reactants flux on the surface. In fig. 21.14, the NO production rate pulse at various crystal temperatures, following the onset of the 5 ms wide $NH_3$ pulse is shown. These traces are

obtained by tuning the laser wavelength to the band head of the $P_{21} + O_{11}$ rovibronic branch of the $A^2\Sigma^+(v'' = 0) \leftarrow X^2\pi_{1/2}(v'' = 0)$ transition of the NO molecule near 225 nm. The second photon of the same wavelength ionizes the NO and the ions current is detected by an electron multiplier.

It was found that at least two different decay curves are observed, representing two NO production mechanisms. The slow and the fast mechanisms had a different temperature dependence as indicated by the two slopes of the corresponding Arrhenius plots. Activation energies of 50 and 121 KJ/mole could be assigned to the slow and the fast reaction mechanisms respectively.

By rotating the optical detector around the sample, an angular distribution, which is also vibrationally and rotationally resolved, was obtained. In fig. 21.15 the angular distribution of ground vibrational state NO product at the band head of the $P_{21} + O_{11}$ transition (including J = ½ to 15/2 rotational states) is shown. It is seen that the NO product angular distribution changes as $\cos^n\theta_f$ where $\theta_f$ is the scattered angle and n = 3/2.

Tuning the laser wavelength around 225 nm, the rotational states distribution within the ground vibrational state was measured. By moving the laser wavelength to the 236 nm range the first vibrationally excited state of the ground electronic state of NO could be monitored as well (Asscher et al., 1983). This way and by carefully calibrating the signal intensity from the ground and the first vibrationally excited molecules, the vibrational distribution of the product NO molecules was obtained. From these measurements it was found that the NO products' rotational states distribution was Botzmann but at a temperature much lower than the crystal temperature. At crystal temperature of 804 K, the rotational temperature was only 340±60 K.

This is even colder than the value obtained for NO scattered from clean pt(111) (Asscher et al., 1983). Similar results were obtained for the vibrational excitation, where a vibrational temperature of 660±70 K was measured.

The results of the reaction rate and the internal state distributions of the NO product led to the conclusion that none of the reaction exothermicity in the gas phase is observed in the product. This means that NO is formed by a Langmuir-Hinschellwood mechanism in which the NO product is adsorbed at the surface prior to desorption and possibly its desorption step is the rate determining of the entire surface reaction. Two mechanisms were suggested to account for the two different decay curves observed with the two different activation energies: One involves the surface reaction between $O_{ad}$ and $N_{ad}$ to form $NO_{ad}$ which then desorbs which is believed to be the slower mechanism with an activation energy of 59 KJ/mole. The second mechanism suggested is the reaction between $NH_{ad}$ and $O_{ad}$ to form $NO_{ad}$ and $H_{ad}$. The overall rate of this mechanism is determined by the desorption of the NO product which determines the activation energy of 121 KJ/mole observed for this fast mechanism, Asscher et al. 1984. The low internal energy content of the product NO molecules is thought to support such a mechanism.

Both studies that were described here, the oxidation of deuterium to produce $D_2O$ and the oxidation of ammonia to form NO are quite complicated surface reactions. They were given as examples of studies which gave information about energy content of products in heterogeneously catalyzed reactions with the hope to understand better the reaction mechanism. Although there is no doubt that this information is of great importance in scrutinizing complicated

surface reactions' mechanisms, it should be stressed that since it was impossible to monitor the surface intermediates in situ with the reaction, the conclusions on the reaction mechanism stay somewhat speculative.

21.4.3 - HIGH ENERGY BEAM: SURFACE-COLLISION INDUCED DISSOCIATION

In a recent theoretical study Elber and Gerber (1983) have predicted the angular and velocity distributions of fragments of a diatomic molecule following high energy impact collisions with a rigid, non vibrating surface. They have used classical trajectry computations for incident $I_2$ and $Ar_2$ beams, having kinetic energies in the range 1-9 eV, impinging upon a diamond surface. The model interaction potential was the surface "dumbbell model" in which the interaction is taken as the sum of each atom-surface potential. The results of these calculations have demonstrated the sensitivity of the resulted fragments' angular and velocity distributions to the details of the interaction potential of the incident molecules with the surface. In the case of soft repulsive part of the potential, a dissociation rainbow effect was found in the angular distribution of the fragments, while a broad distribution was obtained for a very steep repulsive potential (Elber et al., 1983). The velocity distributions predicted for the fragments after collision with these two surfaces were either double maxima or a narrow and single maximum distribution for the soft and steep repulsive potentials respectively. This study was followed by two mechanistic papers by these authors in which they have interpreted the results of the classical trajectories study (Gerber et al., 1984 and Elber et al., 1985).

The role of a centrifugal dissociation mechanism (very high rotational

excitation) as the dominant source for these impact surface mediated dissociation events, (Gerber et al., 1984), and the possibility of having multiple collisions during such impact collision and their effect, (Elber et al., 1985), were discussed.

Parallel to the appearance of these theoretical predictions, an experimental apparatus was set up by Kolodney and Amirav (1983), to study just this type of problems. They have set up a molecular beam machine in which heavy molecules such as iodine, were supersonically expanded through a 30 μm pt orifice (to stand the corrosive $I_2$ gas) via two stages of differential pumping. The iodine molecules were seeded in helium or hydrogen and the nozzle could be heated in such a way that the iodine molecules could have up to 10 eV of kinetic energy. The beam then propagated into a UHV chamber, base pressure of ca. $5 \times 10^{-8}$ pa, and collided with inert but hard surfaces such as the (0001) surface of a saphire single crystal. By having a quadrupole mass spectrometer (QMS) at a fixed angle of $45^{o}$ to the beam axis, they could measure the response of the $I_2^+$ and the $I^+$ signals as a function of the angle between the beam and the normal to the surface, by rotating the sample with respect to the beam axis. Fig. 21.16 shows the angular response of these two signals at two different incident $I_2$ kinetic energies. It is clear that the $I^+$ signal increases rapidly with the incident molecular kinetic energy. By a careful calibration of the $I^+$ signal sources, either from the surface dissociation or from the electron impact in the QMS ionizer they could come up with the dissociation probability. On sapphire they obtained surface-dissociation probabilities of up to 31 percent. This probability varied with the incident beam kinetic energy ($E_K$) as $P = 0.514\ (E_K - E_D)^2$, where $E_D$ is the iodine bond energy of 1.54 eV.

The same experiments of $I_2$ scattering at high energies were performed also on the softer surface of MgO, Kolodney and Amirav, 1984. Here, higher dissociation probabilities were measured as compared with the sapphire surface. Unlike the sapphire surface, the scattering from the MgO exhibited a clear surface temperature dependence, with enhanced dissociation at higher surface temperatures (Kolodney et al., 1984). Kolodney, Amirav, Elber and Gerber (1984) have shown that the dissociation probabilities of $I_2$ on MgO could well be fitted by the classical trajectory calcualtions which are based on the centrifugal mechanism. Fig. 21.17 demonstrates the experimental and theoretical results for the $I_2$ dissociation probability on MgO. It is seen that the experimental results fall in between the rigid surface calculations in which only little energy transfer to the surface was considered, and the non rigid surface, where substantial energy transfer to the surface was allowed.

Finally, time of flight measurements of the scattered $I_2$ molecules, (Kolodney et al., 1984), were performed in order to have an estimation to the extent of energy transfer during a single collision of such heavy molecules with the rigid surfaces. A surprisingly large kinetic energy transfer to the solid during a single collision was found, although the scattered beam was kept supersonic in nature (narrow velocity distribution). The supersonic nature of the scattered beam implies the negligible, if any, contribution to the energy loss from trapping desorption scattering mechanism. The large energy transfer, of up to 6 eV at incident kinetic energy of 9.8 eV, is

attributed to an irreversible traveling compression wave into the solid at the instant in which the $I_2$ center of mass is completely stopped at the solid's surface (Kolodney et al., 1984).

The interesting results discussed above, describing the new phenomena of high energy neutral molecule-surface collisions still await further experimental and theoretical refinements in order to fully understand the results. The differences in the results obtained from the MgO and the sapphire surfaces need further study both theoretically and experimentally. More experimental data, such as the rotational state distribution of the scattered $I_2$ molecules (as a proof of the suggested centrifugal dissociation mechanism) and the fragment I atom velocity distribution are necessary experimental data for the confirmation of the suggested dissociation and energy transfer mechanisms.

## 21.5 - CONCLUDING REMARKS:

Reactive molecular beam surface scattering techniques have been shown to provide useful information on the kinetics and dynamics of surface catalyzed reactions. Historically, the reactive scattering of modulated effusive beams employing the MBRS analysis techniques, were utilized mostly for the determination of kinetic parameters such as the activation energy and preexponential factors of the primary rate limiting surface reaction steps. The use of supersonic beams have shifted the emphasis to more dynamical aspects of reactive processes at surfaces. The recent utilization of optical techniques for the determination of internal state distributions of scattered products, together with time of flight mass spectrometry analysis enabled

REFERENCES

Asscher, M. Guthrie, W.L. Lin, T.H. and Somorjai, G.A. (1982). Phys. Rev. Lett. 49, 76-9.

Asscher, M. Guthrie, W.L. Lin, T.H. and Somorjai, G.A. (1983). J. Chem. Phys. 78, 6992-7004.

Asscher, M. Guthrie, W.L. Lin, T.H. and Somorjai, G.A. (1984). J. Phys. Chem. 88, 3223-38.

Auerbach, D.J. Pfnur, H.E. Rettner, C.T. Schlaegel, J.E. Lee, J. and Madix, R.J. (1984). J. Chem. Phys. 81, 2515-16.

Balooch, M. Cardillo, M.J. Miller, D.R. and Stickney, R.E. (1984). Surf. Sci. 46, 358-92.

Balooch, M. Siekhaus, W.J. and Olander, D.R. (1984). J. Phys. Chem. 88, 3521-28.

Balooch, M. Siekhaus, W.J. and Olander, D.R. (1984). J. Phys. Chem. 88, 3529-31.

Bernasek, S.L. Siekhaus, W.J. and Somorjai, G.A. (1973). Phys. Rev. Lett. 30, 1202-4.

Bernasek, S.L. and Somorjai, G.A. (1985). J. Chem. Phys. 62, 3149-61.

Bertel, E. Schwaha, K. and Netzer, F.P. (1979). Surf. Sci. 83, 439-52.

Bozso, F. Ertl, G. Grunze, M. and Weiss, M. (1977). J. Catal. 49, 18-41.

Campbell, C.T. Ertl, G. Kuipers, H. and Segner, J. (1980). J. Chem. Phys. 73, 5862-73.

Cardillo, M.J. Ching, C.S.Y. Greene, E.F. and Becker, G.E. (1978). J. Vac. Sci. Technol. 15, 423-28.

Cardillo, M.J. (1981). Annu. Rev. Phys. Chem. 32, 331-57.

Cavanagh, R.R. and King, D.S. (1981). Phys. Rev. Lett. 47, 1829-32.

Ceyer, S.T. and Somorjai, G.A. (1977). Annu. Rev. Phys. Chem. 28, 477-99.

Ceyer, S.T. Siekhaus, W.J. and Somorjai, G.A. (1981). J. Vac. Sci. Technol. 19, 726-32.

Ceyer, S.T. Guthrie, W.L. Lin, T.H. and Somorjai, G.A. (1983). J. Chem. Phys. 78, 6982-91.

Chang, H.-C. and Weinberg, W.H. (1977). J. Chem. Phys. 66, 4176-82.

Chang, H.-C. and Weinberg, W.H. (1977). Surf. Sci. 65, 153-64.

Christmann, K. Ertl, G. and Pignet, T. (1976). Surf. Sci. 54, 365-92.

Comsa, G. David, R. and Schumacher, B.J. (1980). Surf. Sci. 95, L210-16.

Comsa, G. and David, R. (1982). Surf. Sci. 117, 77-84.

Conard, H. Ertl, G. and Kuppers, J. (1978). Surf. Sci. 76, 323--42.

Cox, M.P. Ertl, G. Imbihl, R. and Rustig, J. (1983). Surf. Sci. 134, L517-23.

D'Evelyn, M.P. and Madix, R.J. (1983). Surf. Sci. Rep. 3, 413-95.

Elber, R. and Gerber, R.B. (1983). Chem. Phys. Lett. 97, 4-8.

Elber, R. and Gerber, R.B. (1985). Chem. Phys. 92, 363-79.

Engel, T. (1978). J. Chem. Phys. 69, 373-85.

Engel, T. and Ertl, G. (1978). J. Chem. Phys. 69, 1267-81.

Engel, T. and Ertl, G. (1982). In The Chemical Physics of Solid Surface and Heterogeneous Catalysis (eds. D.A. King and D.P. Woodruff) Vol. 4, pp. 73-93. Elsevier, New York.

Ertl, G. Norton, P.R. and Rustig, J. (1982). Phys. Rev. Lett. 49, 177-80.

Ettinger, D. Honma, K. Keil, M. and Polyanzi, J.C. (1982). Chem. Phys. Lett. 87, 413-16.

Fair, J.A. and Madix, R.J. (1980). J. Chem. Phys. 73, 3486-91.

Farnaan, M.K. and Olander, D.R. (1984). Surf. Sci. 145, 390-406.

Foxon, C.C. Bouetry, M.R. and Joyce, B.A. (1974), Surf. Sci. 44, 69-92.

Frenkel, F. Hager, J. Krieger, W. Walther, W. Campbell, C.T. Ertl, G. Kuipers, H. and Segner, J. (1981), Phys. Rev. Lett. 46, 152-55.

Gale, R.J. Salmeron, M. and Somorjai, G.A. (1977). Phys. Rev. Lett. 38, 1027-29.

Gdowski, G.E. and Madix, R.J. (1982). Surf. Sci. 115, 524-40.

Gdowski, G.E. Fair, J.A. and Madix, R.J. (1983). Surf. Sci. 127, 541-54.

Gelb, A. and Cardillo, M.J. (1978). Surf. Sci. 75, 199-214.

Gerber, R.B. and Elber, R.E. (1984). Chem. Phys. Lett. 107, 141-44.

Goddard, P.J. and Lambert, R.M. (1977). Surf. Sci. 67, 180-94.

Gland, J.L. and Kollin, E.B. (1983). J. Chem. Phys. 78, 963-74.

Guthrie, W.L. Sokol, J.D. and Somorjai, G.A. (1981). Surf. Sci. 109, 390-418.

Hayden, J.S. and Diebold, G.J. (1982). J. Chem. Phys. 77, 4767-73.

Hepburn, J.W., Northrup, E.J. Ogram, G.L. Polanyi, J.C. and Williamson, J.M. (1982). Chem. Phys. Lett. 85, 127-30.

Hurst, J.E. Becker, C.A. Cowin, J.P. Janda, K.C. Wharton, L. and Auerbach, D.J. (1979). Phys. Rev. Lett. 43, 1175-77.

Janda, K.C. Hurst, J.E. Cowin, J. Wharton, L. and Auerbach, D.J. (1972). J. Vac. Sci. Technol. 9, 1429-41.

King, D.S. and Cavanagh, R.R. (1982). J. Chem. Phys. 76, 5634-36.

Kitson, M. and Lambert, R.M. (1980). Surf. Sci. 100, 368-80.

Kleyn, A.W. Luntz, A.C. and Auerbach, D.J. (1981). Phys. Rev. Lett. 47, 1169-72.

Kolodney, E. and Amirav, A. (1983). J. Chem. Phys. 79, 4648-50.

Kolodney, E. and Amirav, A. (1984). In Dynamics on Surfaces (eds. B. Pullman, J. Jortner, A. Nitzan and B. Gerber). pp. 231-42.. D. Reidel Publishing Company, Dordrecht.

Kolodney, E. Amirav, A. Elber, R. and Gerber, R.B. (1984). Chem. Phys. Lett. 11, 366-71.

Lee, J. Madix, R.J. Schlaegel, J.E. and Auerbach, D.J. (1984). Surf. Sci. 143, 626-38.

Levkoff, L. Robertson, Jr. A. and Bernasek, S.L. (1984). In Dynamics on Surfaces (eds. B. Pullman and J. Jortner) pp. 243-56. D. Reidel Publishing Company, Dordrecht.

Lin, T.H. (1983). Ph.D. Thesis, University of California, Berkeley.

Lin, T.H. and Somorjai, G.A. (1984). J. Chem. Phys. 81, 704-09.

Luntz, A.C. Kleyn, A.W. and Auerbach, D.J. (1982). J. Chem. Phys. 76, 737-8.

Machiels, A.J. and Olander, D.R. (1977). Surf. Sci. 65, 325-44.

Mantell, D.A. Ryali, S.B. and Haller, G. (1983). Chem. Phys. Lett. 102, 37-40.

Mantell, D.A. Ryali, S.B. Halpern, B.L. Haller, G.L. and Fenn, J.B. (1981). Chem. Phys. Lett. 81, 185-187.

McClelland, G.M. Kubiak, G.D. Rennagel, H.G. and Zare, R.N. (1981). Phys. Rev. Lett. 46, 831-34.

Merril, R.P. (1970). Catalysis Rev. 115-51.

Olander, D.R. (1969). J. Appl. Phys. 40, 4650-57.

Olander, D.R. (1969). In Structure and Chemistry of Solid Surfaces (ed. G.A. Somorjai) pp. 1-45. Wiley, New York.

Olander, D.R. and Kruger, V. (1970). J. Appl. Phys. 41, 2769-76.

Olander, D.R. Jones, R.H. and Siekhaus, W.J. (1970). J. Appl. Phys. 41, 4388-91.

Olander, D.R. Siekhaus, W. Jones, R. and Schwartz J.A. (1972). J. Chem. Phys. 57, 408-20.

Olander, D.R. Jones, R.H. Schwarz, J.A. and Siekhaus, W.J. (1972). J. Chem. Phys. 57, 421-33.

Olander, D.R. and Ullman, A. (1976). Int. J. Chem. Kin. 8, 625-37.

Olander, D.R. Acharya, T.R. and Ullman, A.Z. (1977). J. Chem. Phys. 67, 3549-62.

Olander, D.R. (1977). J. Coll. Interface Sci. 58, 169-83.

Pacia, N. Cassuto, A. Pentenero, A. and Weber, B. (1976). J. Catal. 41, 455-65.

Palmer, R.L. Smith, Jr. J.N.S. Saltsburg, H. and O'Keefe, D.R. (1970). J. Chem. Phys. 53, 1666-76.

Palmer, R.L. and Smith, Jr. J.N.S. (1974). J. Chem. Phys. 60, 1453-63.

Salmeron, M. Gale, R.J. and Somorjai, G.A. (1977). J. Chem. Phys. 67, 5324-34.

Salmeron, M. Gale, R.J. and Somorjai, G.A. (1979). J. Chem. Phys. 70, 2807-18.

Sawin, H.H. and Merril, R.P. (1981). J. Vac. Sci. Technol. 19, 40-6.

Schwaha, K. Spencer, N.D. and Lambert, R.M. (1979). Surf. Sci. 81, 273-84.

Schwarz, J.A. and Madix, R.J. (1974). Surf. Sci. 46, 317-41.

Segner, J. Campbell, C.T. Doyen, G. and Ertl, G. (1984). Surf. Sci. 138, 505-23.

Siekhaus, W.J. Jones, R.H. and Olander, D.R. (1970). J. Appl. Phys. 41, 4392-403.

Smith, Jr., J.N. and Fite, W.L. (1963). In Proc. Third Inter. Symp. Rarified

Gas Dynamics. Vol. 1, pp. 430.

Smith, Jr., J.N. and Saltzburg, H. (1964). J. Chem. Phys. 40, 3585-91.

Smith, Jr., J.N. and Palmer, R.L. (1972), J. Chem. Phys. 56, 13-20.

Somorjai, G.A. (1981). Chemistry in Two Dimension: Surfaces. Cornell University Press.

Spencer, N.D. (1980). Ph.D. Thesis. University of Cambridge.

Spencer, N.D. Goddard, P.J. Davis, P.W. Kitson, M. and Lambert, R.M. (1983). J. Vac. Sci. Technol. A1, 1554-5.

Thorman, R.P. and Bernasek, S.L. (1981). J. Chem. Phys. 74, 6498-6504.

Tully, J.C. (1981). Suf. Sci. 111, 461-78.

Turner, J.E. (1982). Ph.D. Thesis, University of California, San Diego.

West, L.A. Kozak, E.I. and Somorjai, G.A. (1971). J. Vac. Sci. Technol. 8, 430-36.

Winterbottom, W.L. (1973). Surf. Sci. 36, 205-24.

Yeates, R.C. Turner, J.E. Gellman, A.J. and Somorjai, G.A. (1985). Surf. Sci. 149, 175-90.

Zacharias, H. Loy, M.M.T. and Roland, P.A. (1982). Phys. Rev. Lett. 49, 1790-4.

## Figure Captions

21.1 A molecular beam surface scattering apparatus (from Ceyer et al., 1981).

21.2 A schematic of an optical detection via multiphoton ionization of scattered molecules from surfaces.

21.3 Molecular chlorine electrochemical source (from Spencer et al., 1983).

21.4 Polar plots of the product reaction vector ($\epsilon$) for: (a) a simple adsorption/desorption reaction; (b) a two step reaction sequence with $k_1 = k_2 = k$ and (c) a parallel branched reaction (from Jones et al., 1972).

21.5 Angular distribution of hydrogen, deuterium and hydrogen deuteride for the three surfaces: a) Pt(111); b) Pt(997) or Pt(S)-[9(111)x(111)] and c) Pt(553) or Pt(s)-[5(111)x(111)], (from Bernasek and Somorjai, 1975).

21.6 HD production as a function of angle of incidence $\theta$, of the molecular beam, normalized to the incident $D_2$ intensity. The expression in the parenthesis is a correction factor which accounts for the relative proportions of $H_2$ and $D_2$ in the beam as explained in section 5.4 (Salmeron et al., 1977). a) Pt(332) or Pt(S)-[6(111)x(111)] surface, with the step edges perpendicular to the incident beam ($\phi = +90^o$), b) Pt(332) where the projection of the beam on the surface is parallel to the step edges ($\phi = 0^o$), c) Pt(111) surface (from Salmeron et al., 1977).

21.7 a) HD production on the Pt(332) surface as a function of azimuthal angle, $\phi$, normalized to the incident $D_2$ intensity. The expression in paranthesis is explained in fig. 6. The solid line is a sine function

fit to the data in order to perform the integration discussed in section 5.4 of Salmeron et al. 1977.

21.8 Arrhenius plots of the effective rate constant for hydrogen evolution following decomposition of $D_2CO$ on pt(S)-[9(111)x(100)]: a) Without CO beam and b) With a CO beam flux of $10^{15}$ $cm^2 \cdot sec^{-1}$ (from Gdowski et al., 1983).

21.9 Apparent reaction probability and phase lag of $PbCl_2$ as a function of target temperature (from Balooch et al., 1984).

21.10 Response of electrochemical chlorine gun to driving waveforms of varying harmonic content (from Spencer, 1980).

21.11 Initial sticking probability $S_o$, as a function of translational energy of $N_2$ molecules incident on a W(110) surface at various angles of incidence. It is seen that $S_o$ is insensitive to $\theta_i$ for $\theta_i < 45^o$. The dashed curve indicates the sticking probability predicted at $\theta_i = 60^o$ by using $\theta_i = 0^o$ data and assuming that $S_o$ scales with the normal component of the kinetic energy. The actual $\theta_i = 60^o$ results lie much closer to the uncorrected $\theta_i = 0^o$ data (from Lee et al., 1984).

21.12 Enthalpy diagram for the CO oxidation reaction on Pt(111) in low coverage limit (from Campbell et al. 1980).

21.13 $D_2O$ translational energy distributions for: a) $T_s = 913$ K, $\theta = 7^o$; B) $T_s = 870$ K, $\theta = 7^o$; c) $T_s = 765$ K, $\theta = 7^o$ where $\theta$ is the angle of detection measured from the normal to the surface (from Ceyer et al., 1984).

21.14 The rise and decay of the NO (v' = 0) production rate as a function of time, at different crystal temperatures. At the top, the shape of the

incident $NH_3$ beam pulse is shown (from Asscher et al., 1984).

21.15 Angular distribution of the NO (v' = 0) product of the ammonia oxidation on Pt(111). The incident angle $\theta_i$ of the ammonia beam is $64^o$ with the crystal at 804K. The dashed line is a calculated angular distribution with the function $\cos^{3/2}\theta_f$, where $\theta_f$ is the scattering angle from the surface normal (from Asscher et al., 1984).

21.16 The molecular and atomic iodine signal at the QMS detector vs. the surface-beam axis angle. The QMS detector is fixed at $45^o$ to the beam axis while the sapphire surface was rotating. The sapphire single crystal (0001 orientation) was held at $650^oC$. The iodine was seeded with hydrogen and expanded through a 30 μ nozzle. The nozzle temperature was $75^oC$ corresponding to 12 Torr iodine partial pressure. The hydrogen nozzle backing pressure was in Fig. 16(a) 700 Torr resulting in 2.4 eV molecular iodine kinetic energy while in Fig.(B) it was 13,500 Torr resulting in 9.8 eV molecular iodine kinetic energy. The QMS ionizing electron energy was 50 eV (from Kolodney and Amirv, 1984).

21.17 Molecular iodine dissociation probability after a single collision with MgO surface vs. kinetic energy. MgO surface temperature is $275^oC$, nozzle diameter is 30 μ and nozzle temperature is $75^oC$. Both hydrogen and helium (full circles connected by a full line) are used as carrier gases. The upper dashed curve is the classical trajectory calculation results for rigid surface with only little gas-surface energy transfer. The lower curve is the trajectory calculations for a more realistic MgO surface which also exhibits a substantial gas-surface energy transfer (from Kolodney and Amirav, 1984).

# INDEX I


Names

Auger (4)
Arrhenius (12,40)
Maxwellian distribution (7,38)
Languir-Hinshelwood (16,25,28,41)
Eiley-Rideal (16,25,28)

Subjects

Heterogeneous Catalysis (1)
Surface Area (1)
Modulated Beam Relaxation Spectrometry (2,3,10,14,25,26)
Low Energy Electron Diffraction (4)
Quadrupole mass Spectrometer (4)
Laser Induced Flourescence (5)
Multiphoton ionization (5,39,40)
Time of flight (6,37)
Auger Electron Spectroscopy (4)
Electrochemical gun (7,29,30)
Sticking Probability (8,11,14,15)
Activated adsorption (9,31)
Dissociative adsorption (9,11,31,33)
Desorption rate (11)
Residence time (12,37)
Surface transfer function (14)
Supersonic molecular beam (30,42)
Angular distribution (peaked at the normal to the surface) (33,35,37,39,40,42)
Precursor state (33)
Internal energy excitation (35,36)
Deuterium oxidation (36,37)
Ammonia oxidation (36,37,39)
CO oxidation (24,25,26,35,36)
Non-equilibrated desorption (38)
Collision induced dissociation (42)
Traveling compression wave (44)

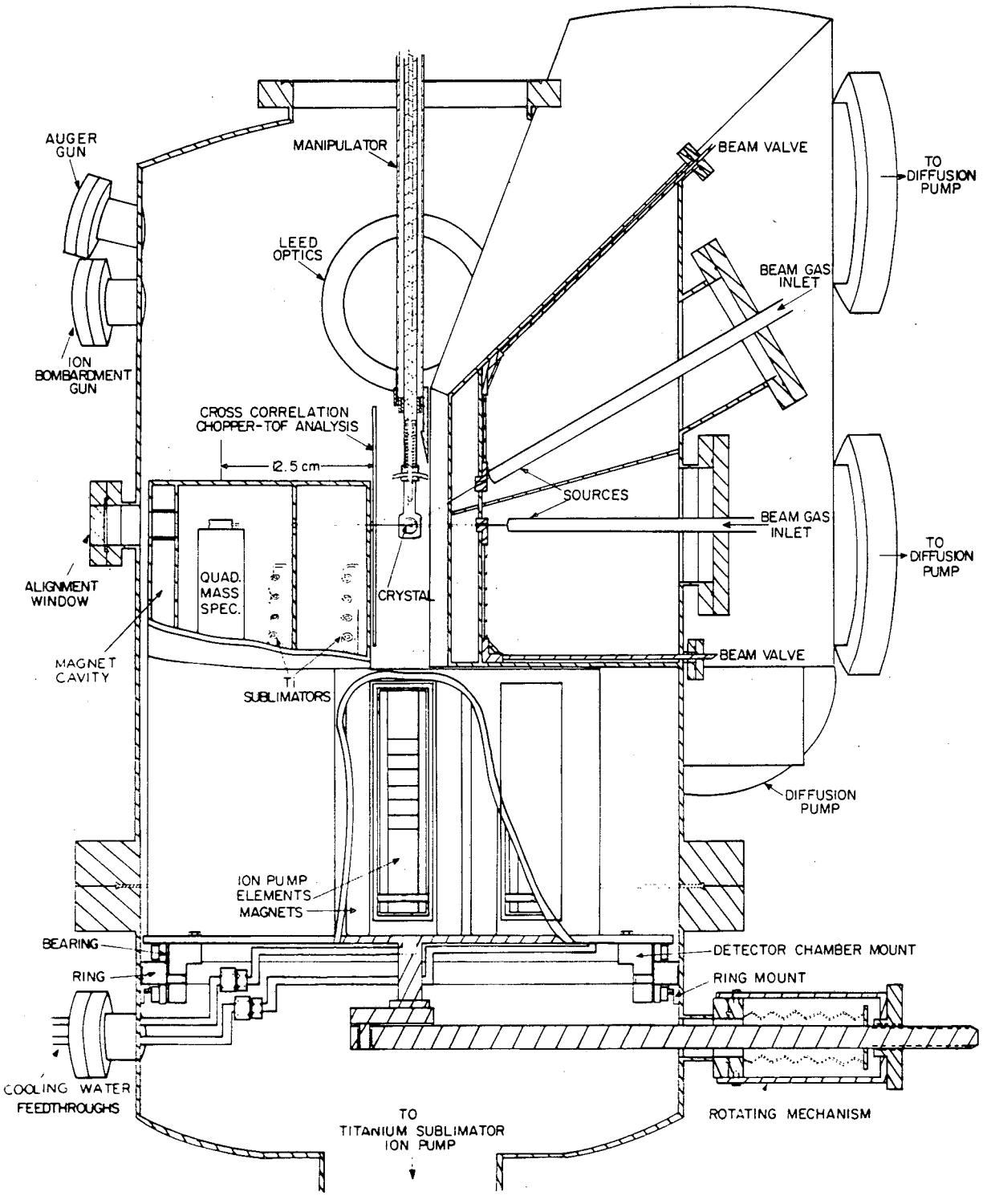
AUGER GUN
MANIPULATOR
BEAM VALVE
TO DIFFUSION PUMP
LEED OPTICS
BEAM GAS INLET
ION BOMBARDMENT GUN
CROSS CORRELATION CHOPPER-TOF ANALYSIS
12.5 cm
SOURCES
BEAM GAS INLET
TO DIFFUSION PUMP
ALIGNMENT WINDOW
QUAD. MASS SPEC.
CRYSTAL
MAGNET CAVITY
BEAM VALVE
Ti SUBLIMATORS
DIFFUSION PUMP
ION PUMP ELEMENTS
MAGNETS
BEARING
DETECTOR CHAMBER MOUNT
RING
RING MOUNT
COOLING WATER FEEDTHROUGHS
TO TITANIUM SUBLIMATOR ION PUMP
ROTATING MECHANISM
XBL 799-11376

Fig. 21.1

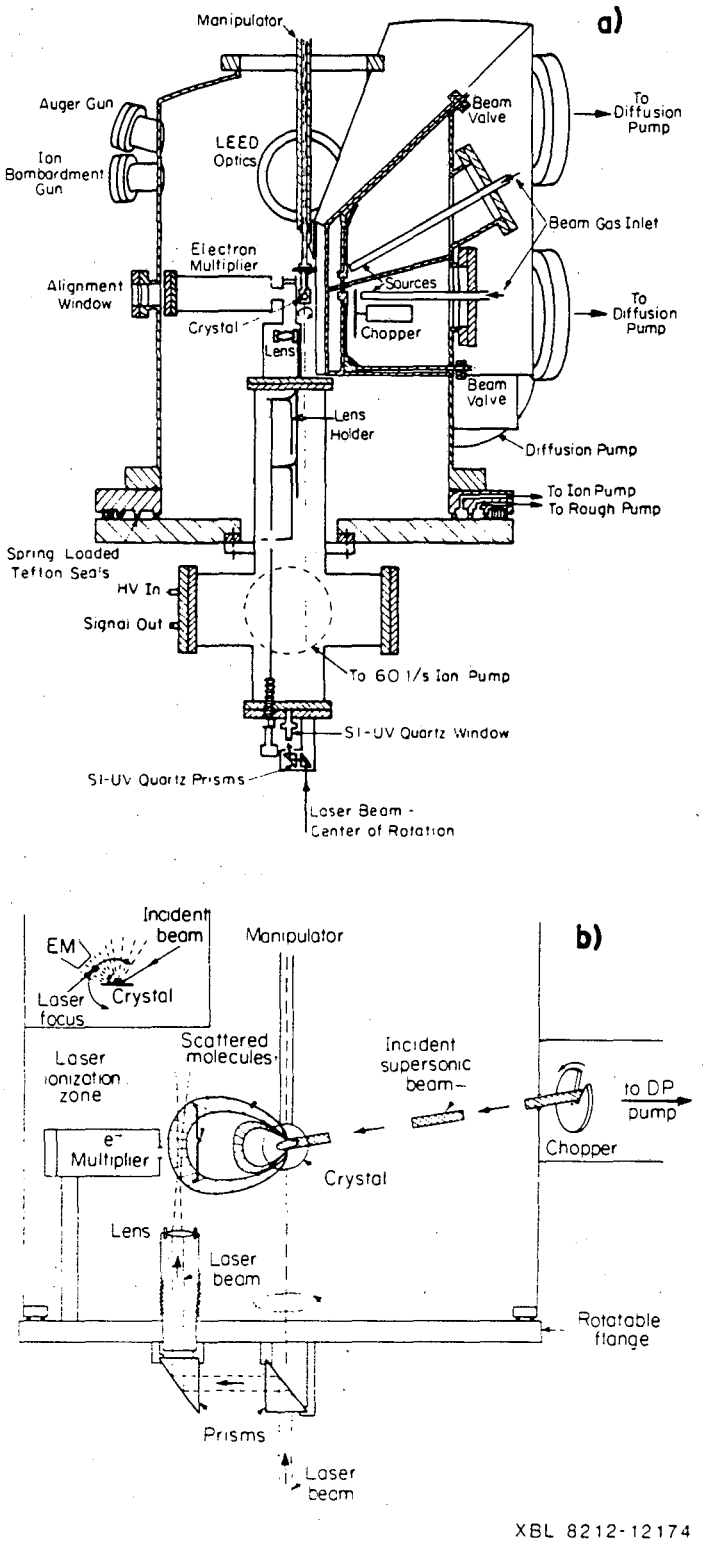
a)
Manipulator
Auger Gun
Ion Bombardment Gun
LEED Optics
Beam Valve
To Diffusion Pump
Beam Gas Inlet
Electron Multiplier
Alignment Window
Sources
Crystal
Chopper
Lens
Beam Valve
Lens Holder
Diffusion Pump
To Ion Pump
To Rough Pump
Spring Loaded Teflon Seals
HV In
Signal Out
To 60 l/s Ion Pump
SI-UV Quartz Window
SI-UV Quartz Prisms
Laser Beam - Center of Rotation
b)
Incident beam
EM
Laser focus
Crystal
Manipulator
Scattered molecules
Laser ionization zone
Incident supersonic beam
to DP pump
e⁻ Multiplier
Chopper
Crystal
Lens
Laser beam
Rotatable flange
Prisms
Laser beam
XBL 8212-12174

Fig. 21.2

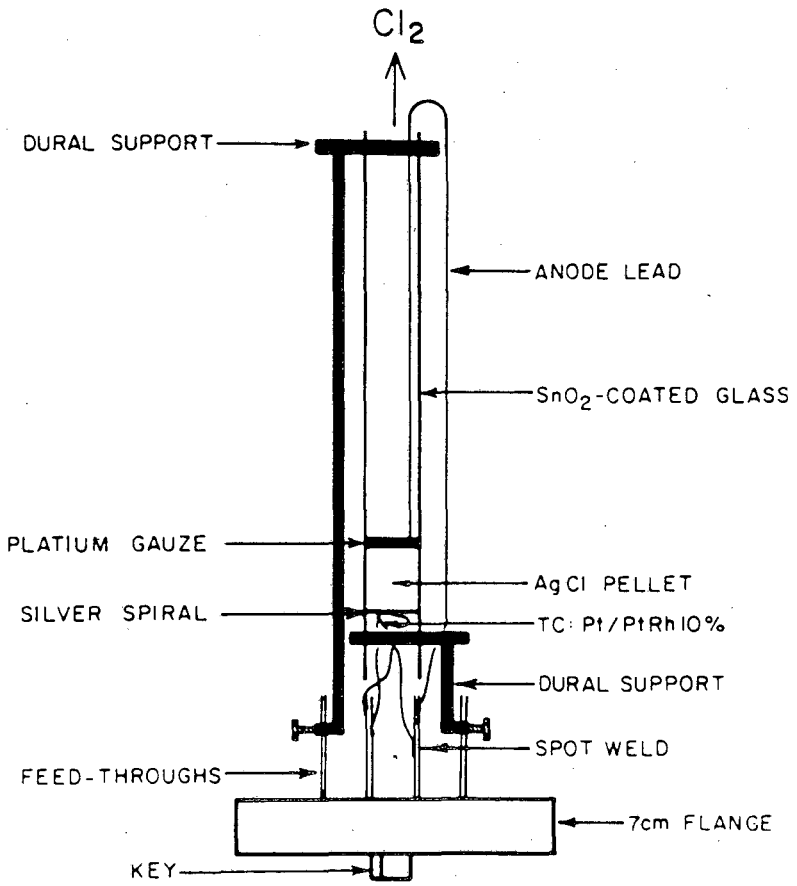
$Cl_2$
DURAL SUPPORT
ANODE LEAD
$SnO_2$-COATED GLASS
PLATIUM GAUZE
AgCl PELLET
SILVER SPIRAL
TC: Pt/PtRh10%
DURAL SUPPORT
SPOT WELD
FEED-THROUGHS
7cm FLANGE
KEY

Fig. 21.3

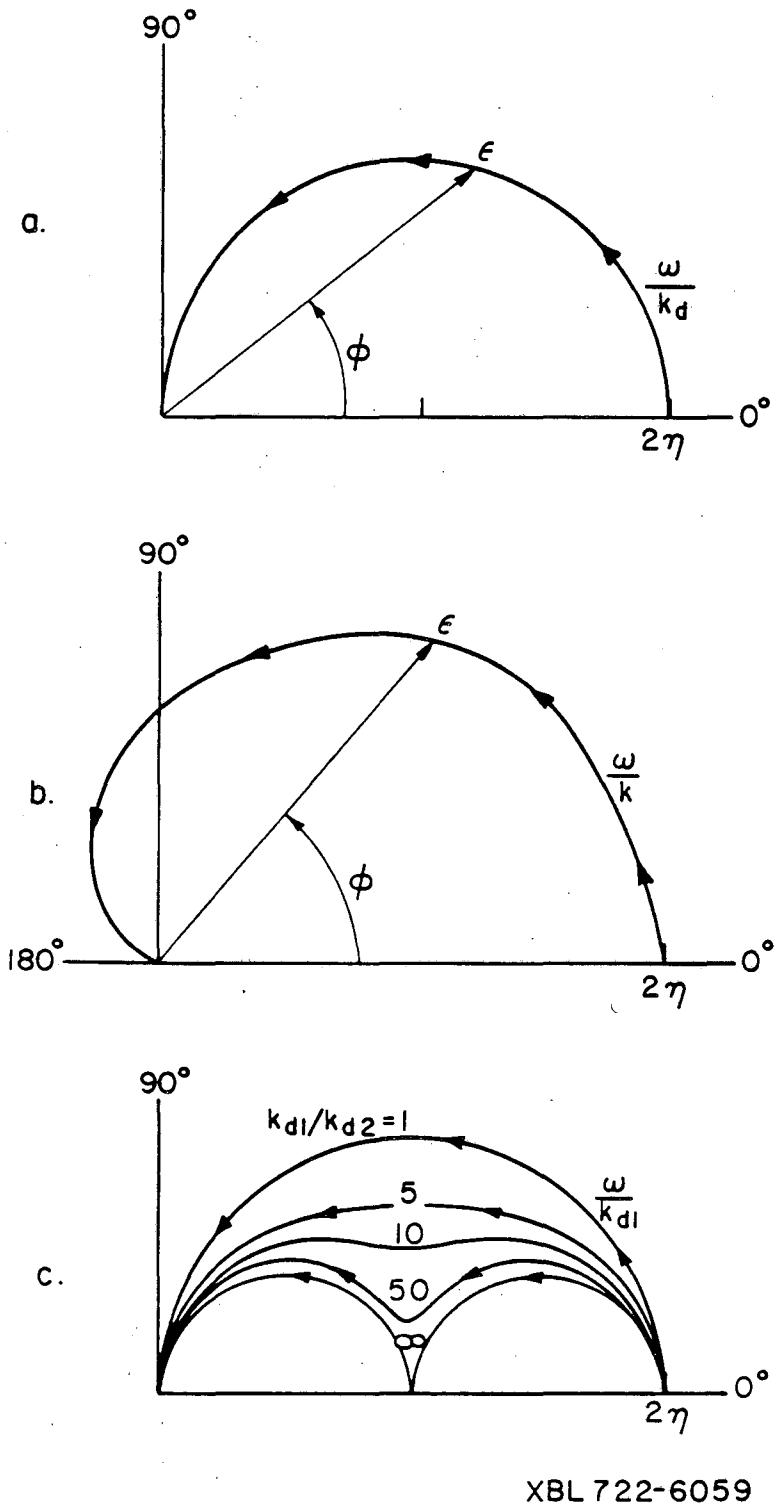


XBL 722-6059

Fig. 21.4

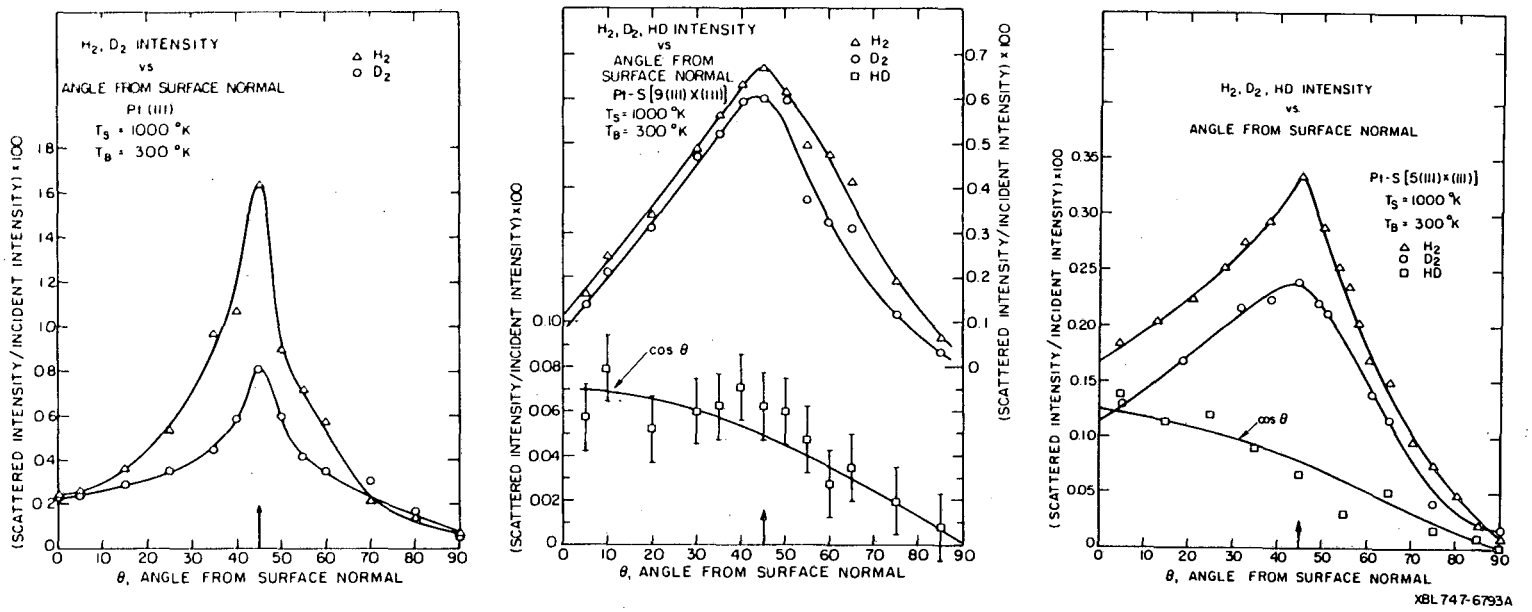
H2, D2 INTENSITY
vs
ANGLE FROM SURFACE NORMAL
Pt (111)
TS = 1000 °K
TB = 300 °K
H2
D2
(SCATTERED INTENSITY/INCIDENT INTENSITY) x 100
θ, ANGLE FROM SURFACE NORMAL
H2, D2, HD INTENSITY
vs
ANGLE FROM
SURFACE NORMAL
Pt-S [9(111) x (111)]
TS = 1000 °K
TB = 300 °K
H2
D2
HD
cos θ
(SCATTERED INTENSITY/INCIDENT INTENSITY) x 100
(SCATTERED INTENSITY/INCIDENT INTENSITY) x 100
θ, ANGLE FROM SURFACE NORMAL
H2, D2, HD INTENSITY
vs.
ANGLE FROM SURFACE NORMAL
Pt-S [5(111) x (111)]
TS = 1000 °K
TB = 300 °K
H2
D2
HD
cos θ
(SCATTERED INTENSITY/INCIDENT INTENSITY) x 100
θ, ANGLE FROM SURFACE NORMAL
XBL 747-6793A

Fig. 21.5

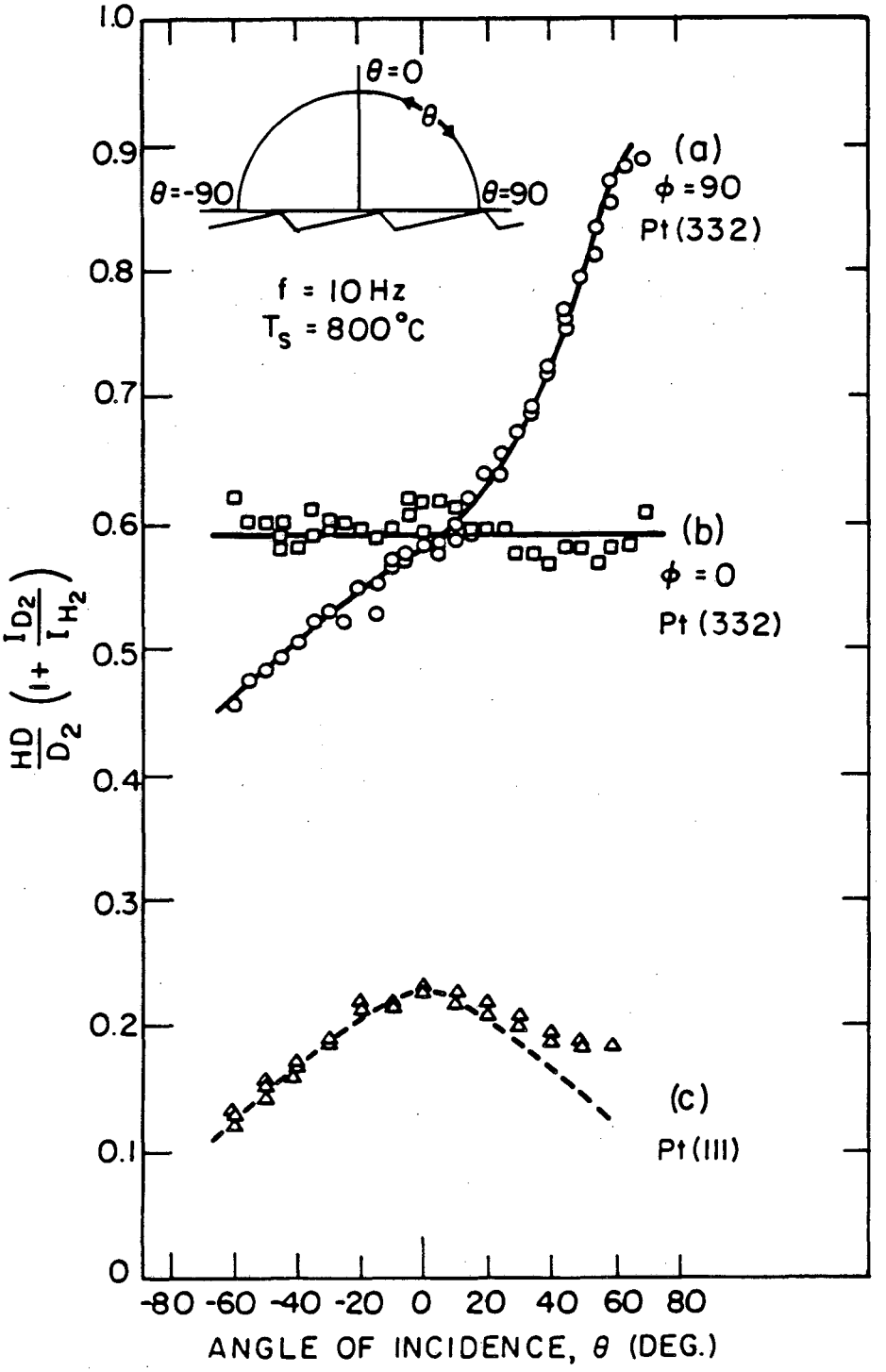


XBL 772-5084A

Fig. 21.6

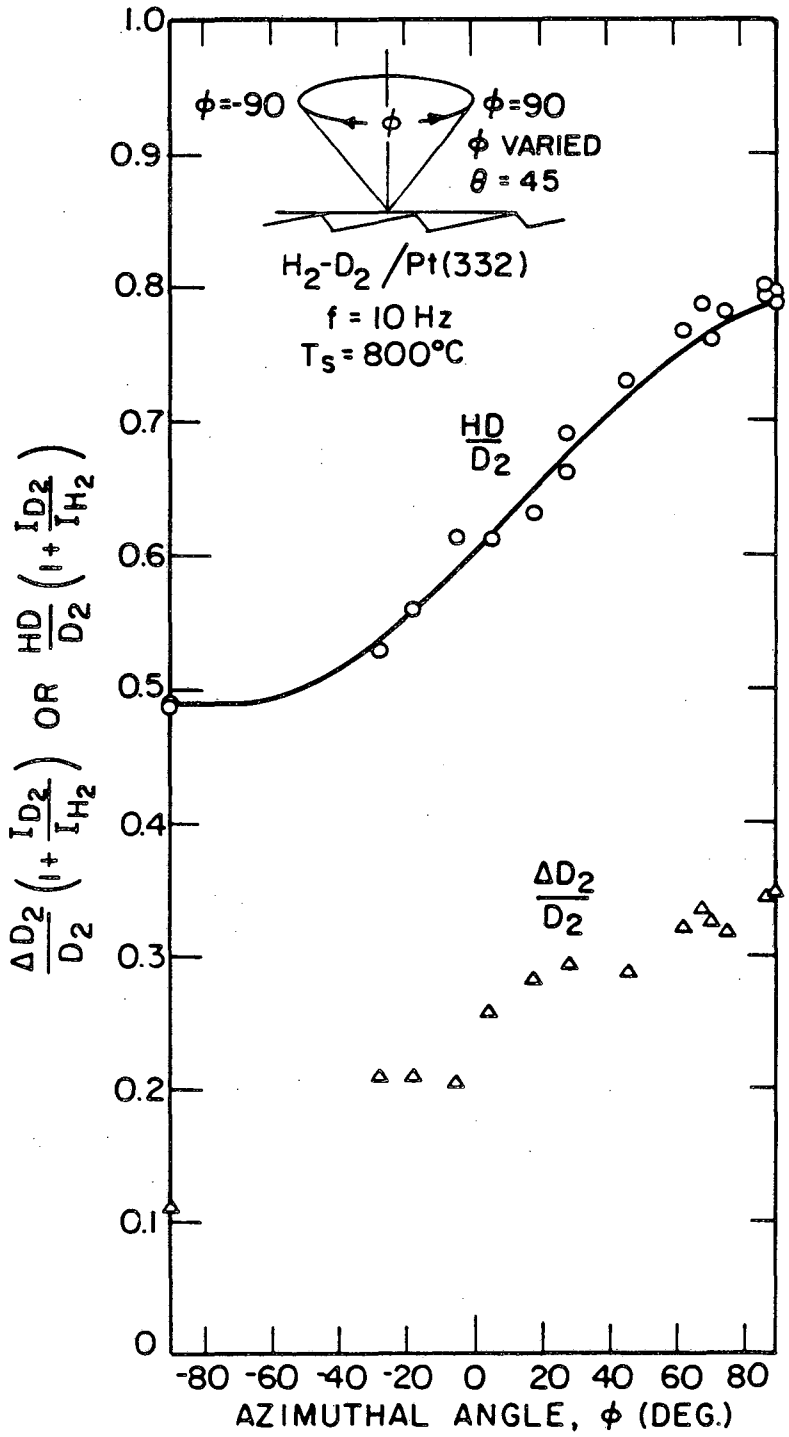


XBL773-5227

Fig. 21.7

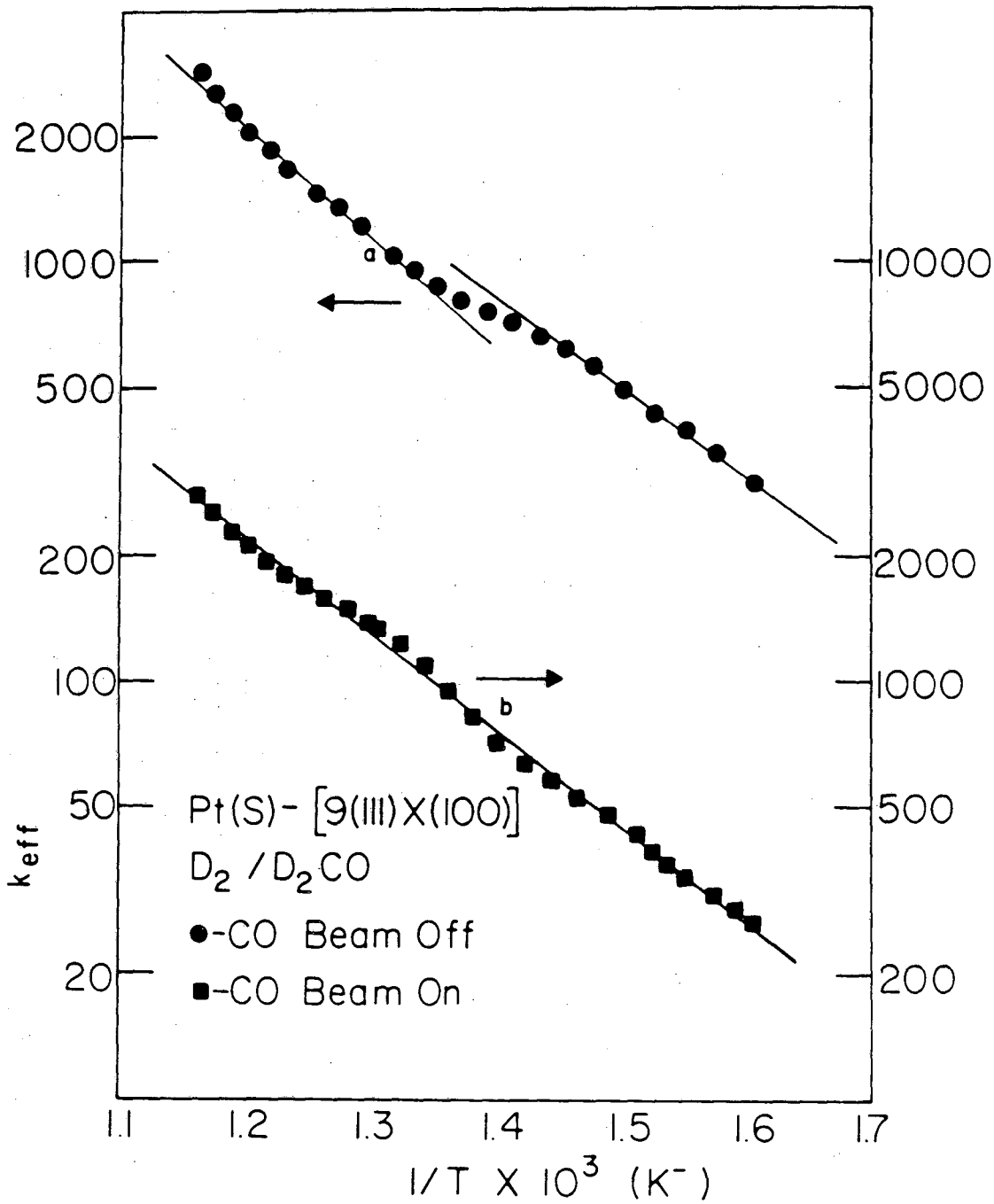
2000
1000
500
200
100
50
20
10000
5000
2000
1000
500
200
a
b
Pt(S)- [9(111)X(100)]
D2 / D2CO
●-CO Beam Off
■-CO Beam On
keff
1.1
1.2
1.3
1.4
1.5
1.6
1.7
1/T X 10^3 (K^-)

Fig. 21.8

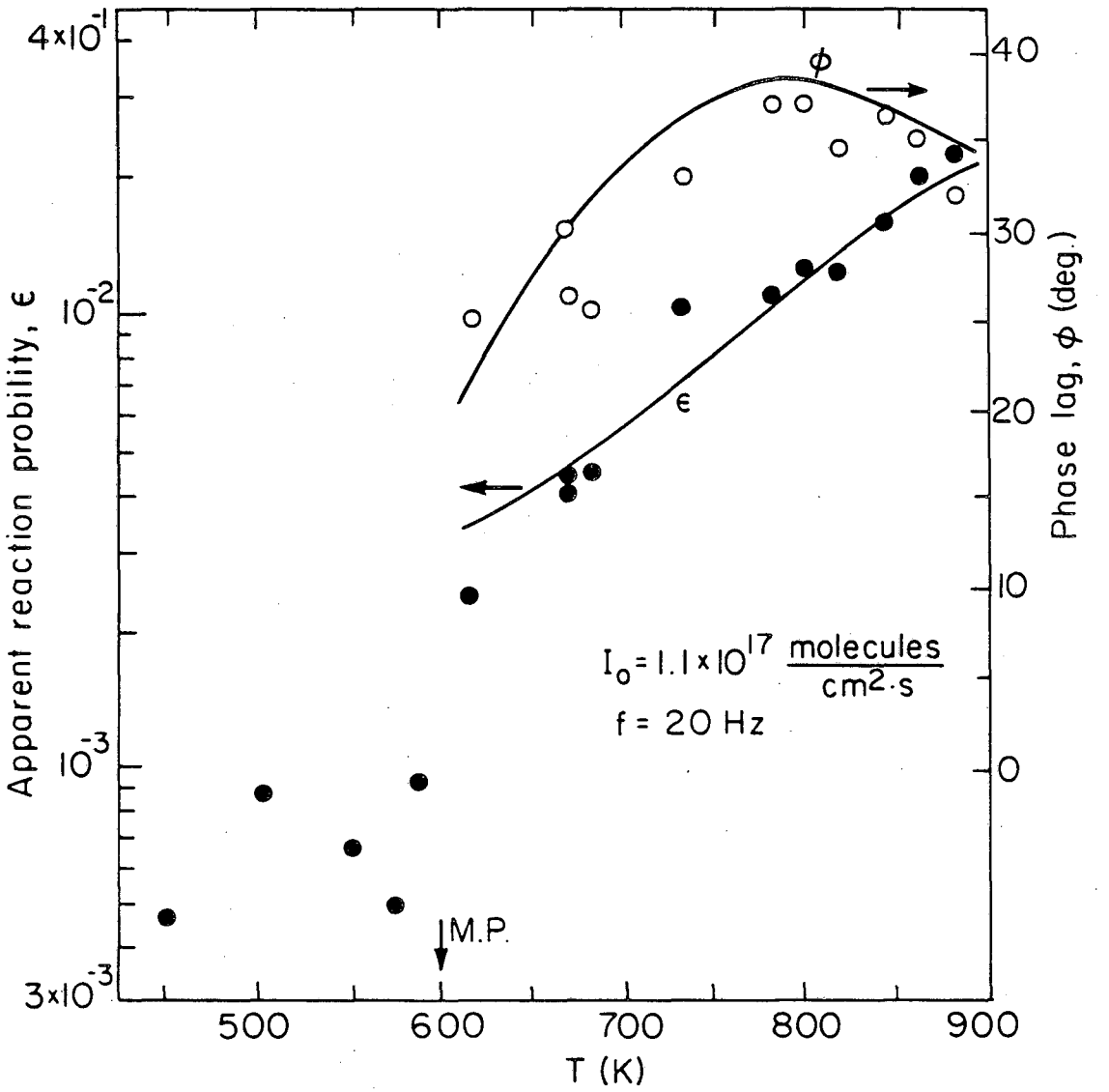
4×10⁻¹
10⁻²
10⁻³
3×10⁻³
Apparent reaction probility, ϵ
40
30
20
10
0
Phase lag, ϕ (deg.)
ϕ
ϵ
I₀ = 1.1 × 10¹⁷ molecules / cm²·s
f = 20 Hz
M.P.
500
600
700
800
900
T (K)
XBL 834-5532

Fig. 21.9

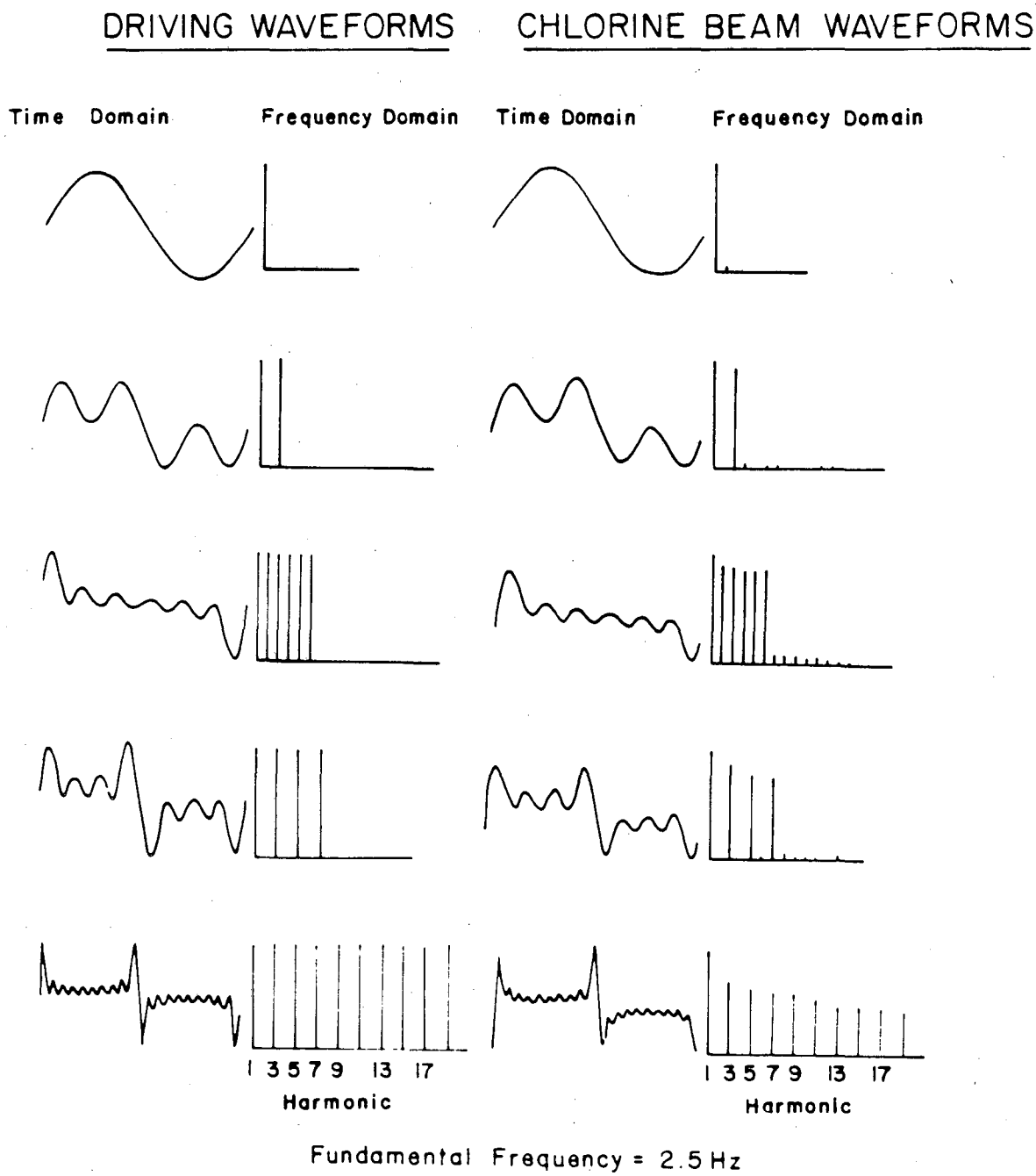
DRIVING WAVEFORMS
CHLORINE BEAM WAVEFORMS
Time Domain
Frequency Domain
Time Domain
Frequency Domain
1 3 5 7 9 13 17
Harmonic
1 3 5 7 9 13 17
Harmonic
Fundamental Frequency = 2.5 Hz

Fig. 21.10

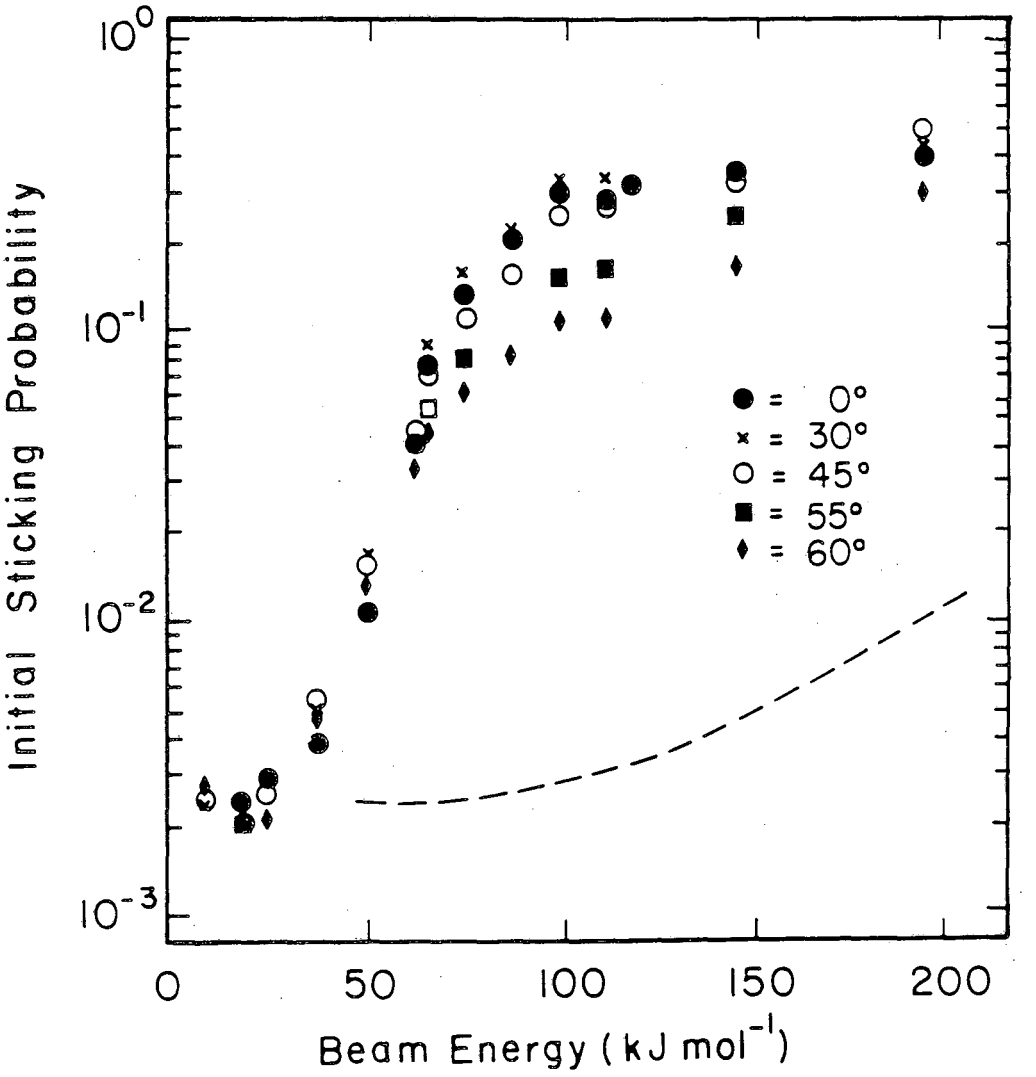
Initial Sticking Probability
$10^0$
$10^{-1}$
$10^{-2}$
$10^{-3}$
0
50
100
150
200
Beam Energy ( kJ mol$^{-1}$)
● = 0°
× = 30°
○ = 45°
■ = 55°
♦ = 60°

Fig. 21.11

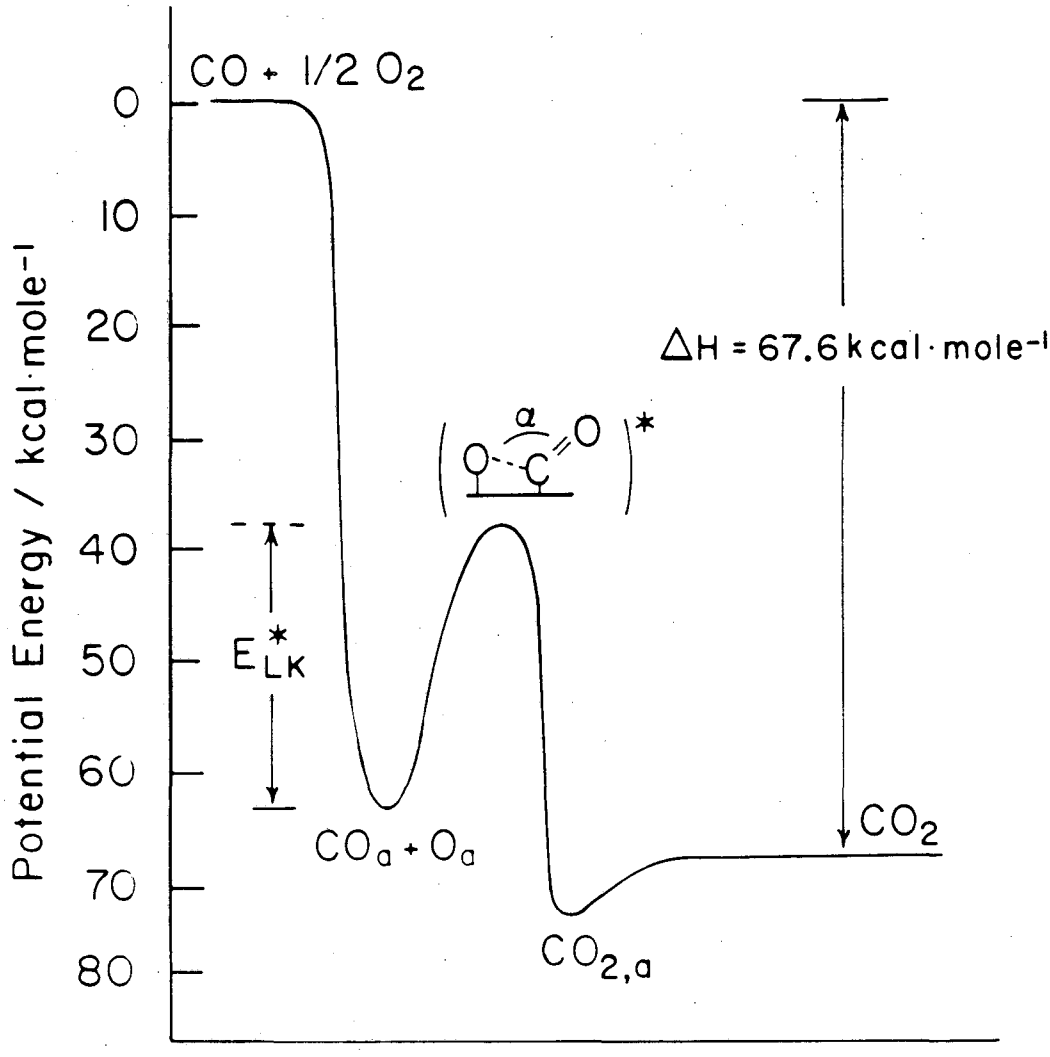
CO + 1/2 O2
0
10
20
30
40
50
60
70
80
Potential Energy / kcal·mole-1
ΔH = 67.6 kcal·mole-1
α
O
O
C
*
E*LK
COa + Oa
CO2,a
CO2

Fig. 21.12

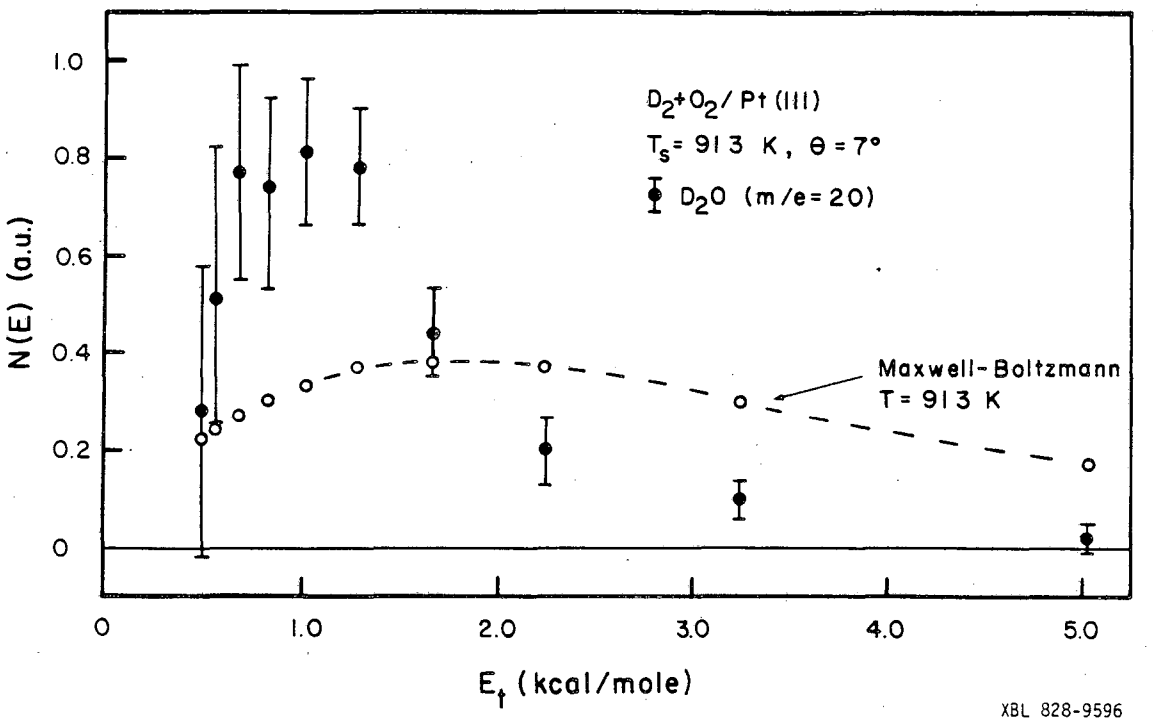
1.0
0.8
0.6
0.4
0.2
0
N(E) (a.u.)
$D_2+O_2$/ Pt (111)
$T_s$= 913 K, θ = 7°
$D_2O$ (m/e=20)
Maxwell-Boltzmann
T= 913 K
0
1.0
2.0
3.0
4.0
5.0
$E_t$ (kcal/mole)
XBL 828-9596

Fig. 21.13a

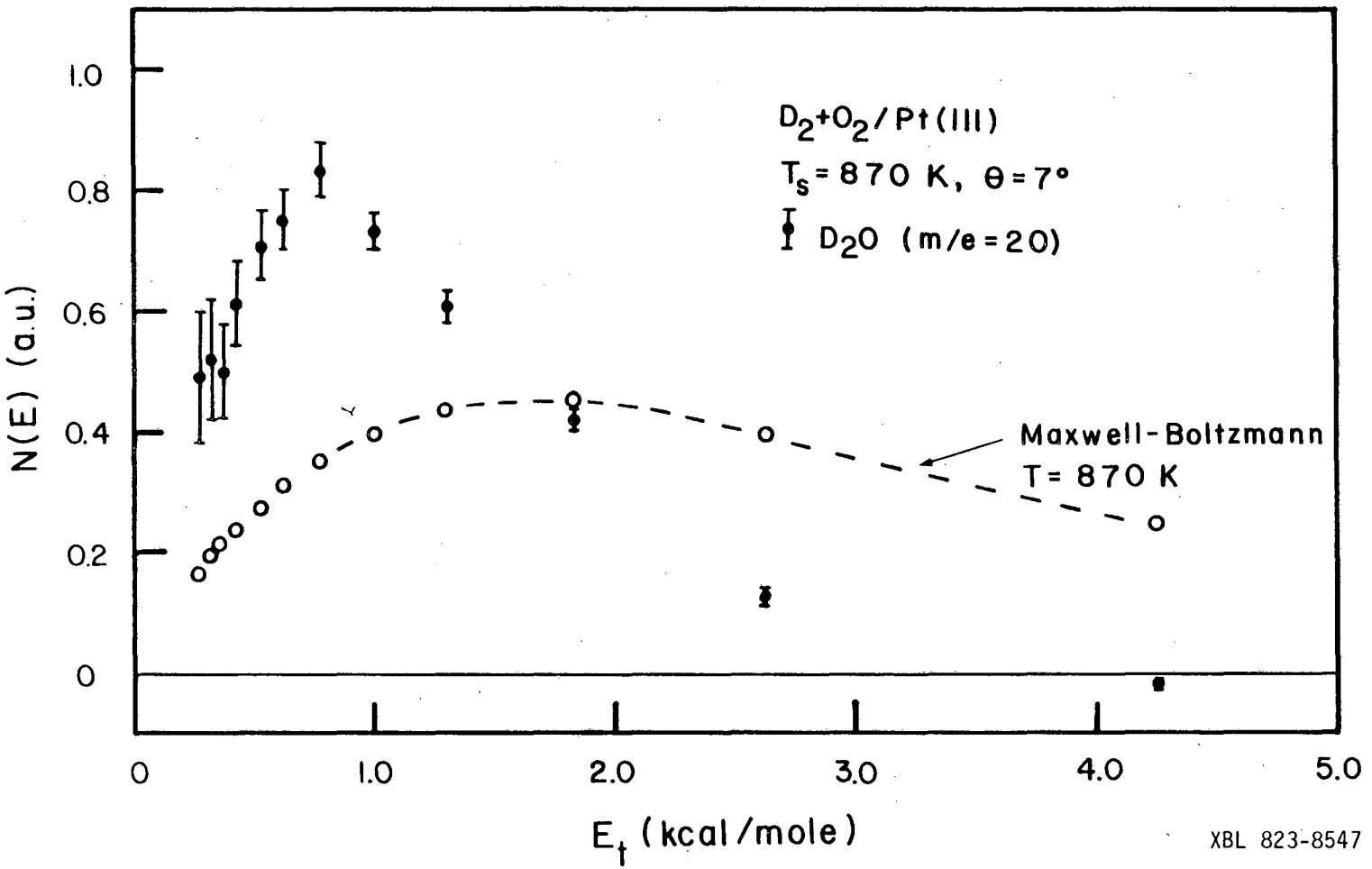
$D_2+O_2/Pt(111)$
$T_s = 870$ K, $\theta = 7°$
$D_2O$ (m/e = 20)
Maxwell-Boltzmann
T = 870 K
N(E) (a.u.)
1.0
0.8
0.6
0.4
0.2
0
0
1.0
2.0
3.0
4.0
5.0
$E_t$ (kcal/mole)
XBL 823-8547

Fig. 21.13b

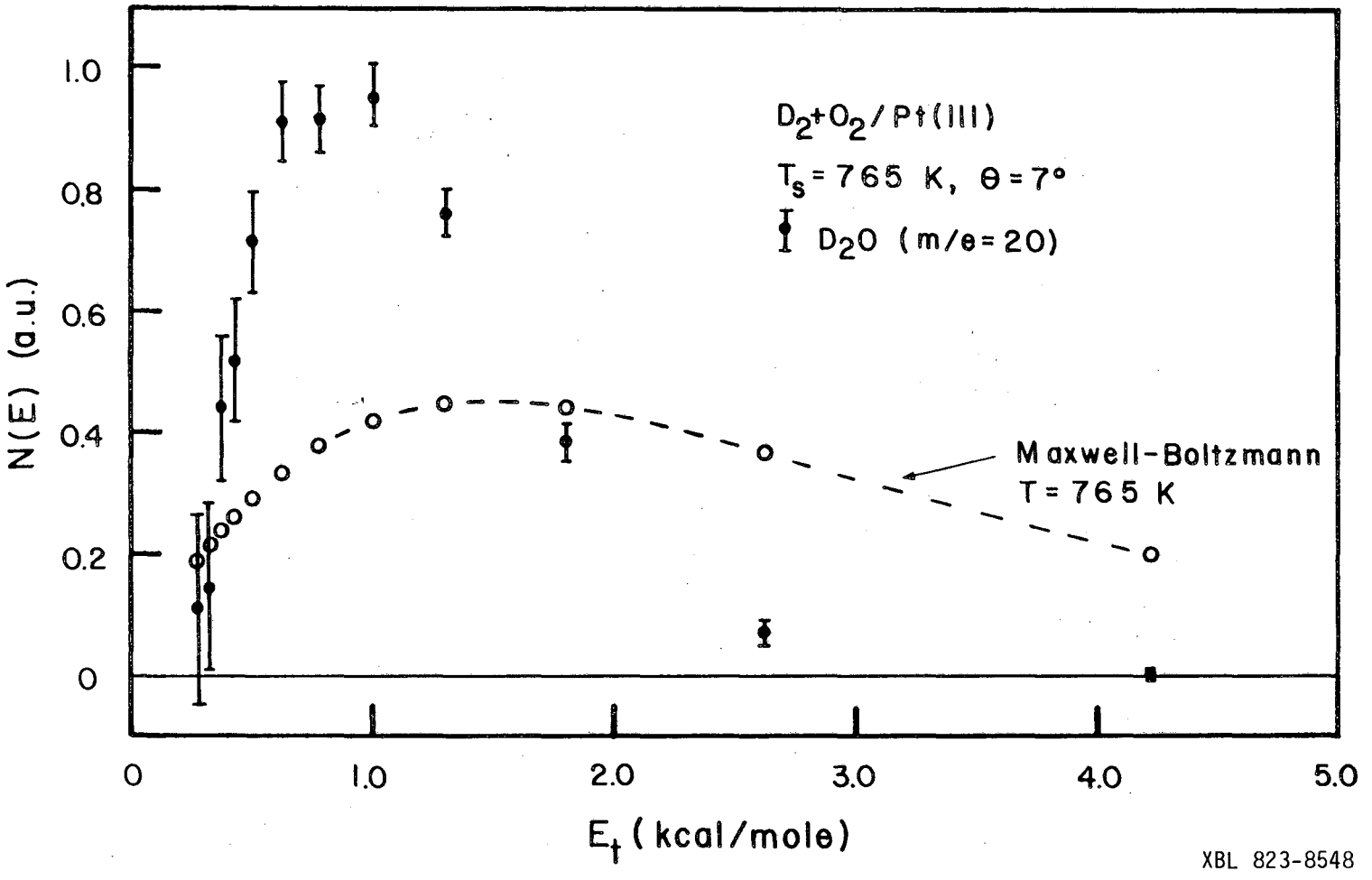


XBL 823-8548

Fig. 21.13c

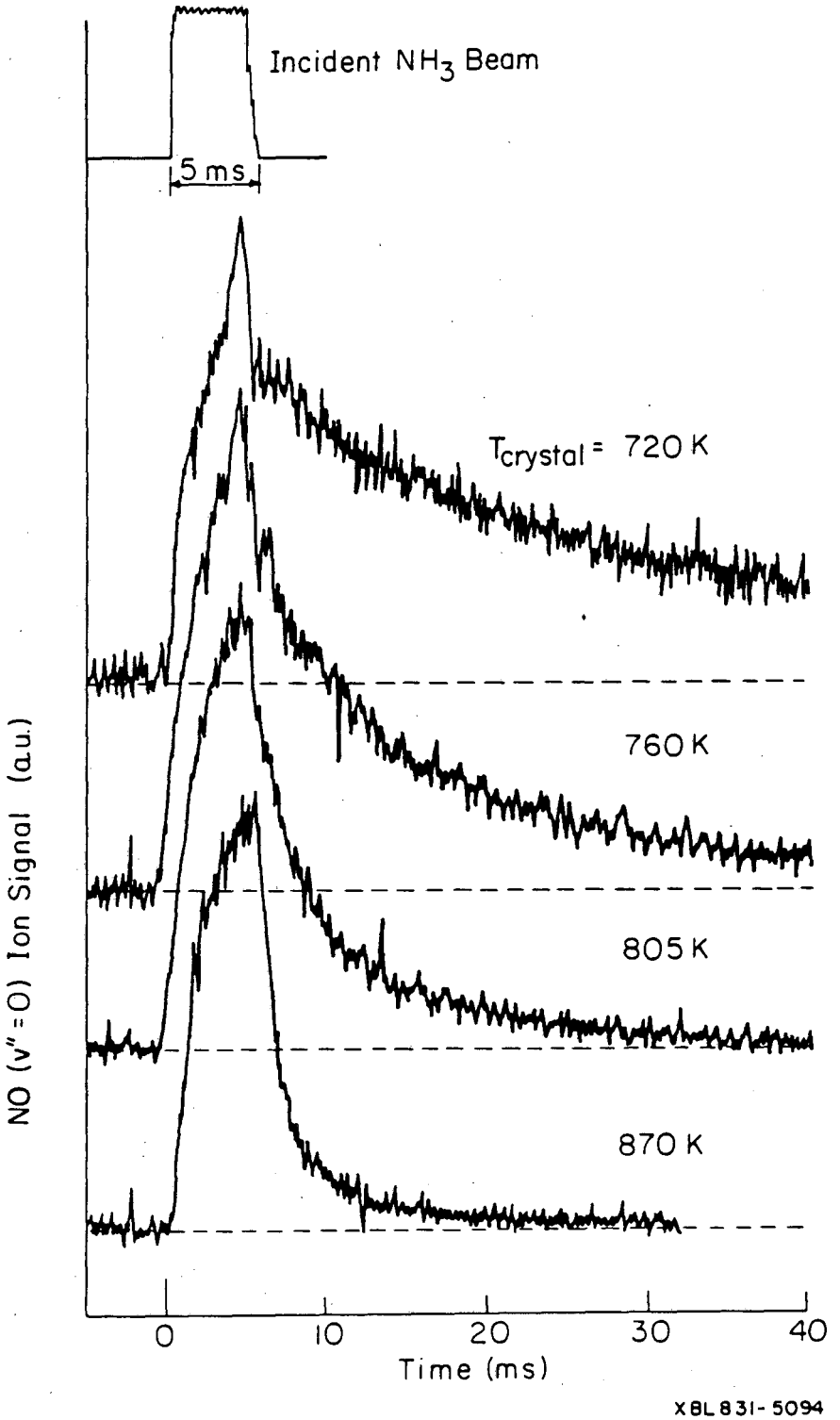
Incident $NH_3$ Beam
5 ms
$T_{crystal}$ = 720 K
760 K
805 K
870 K
NO (v"=0) Ion Signal (a.u.)
0
10
20
30
40
Time (ms)
XBL 831-5094

Fig. 21.14

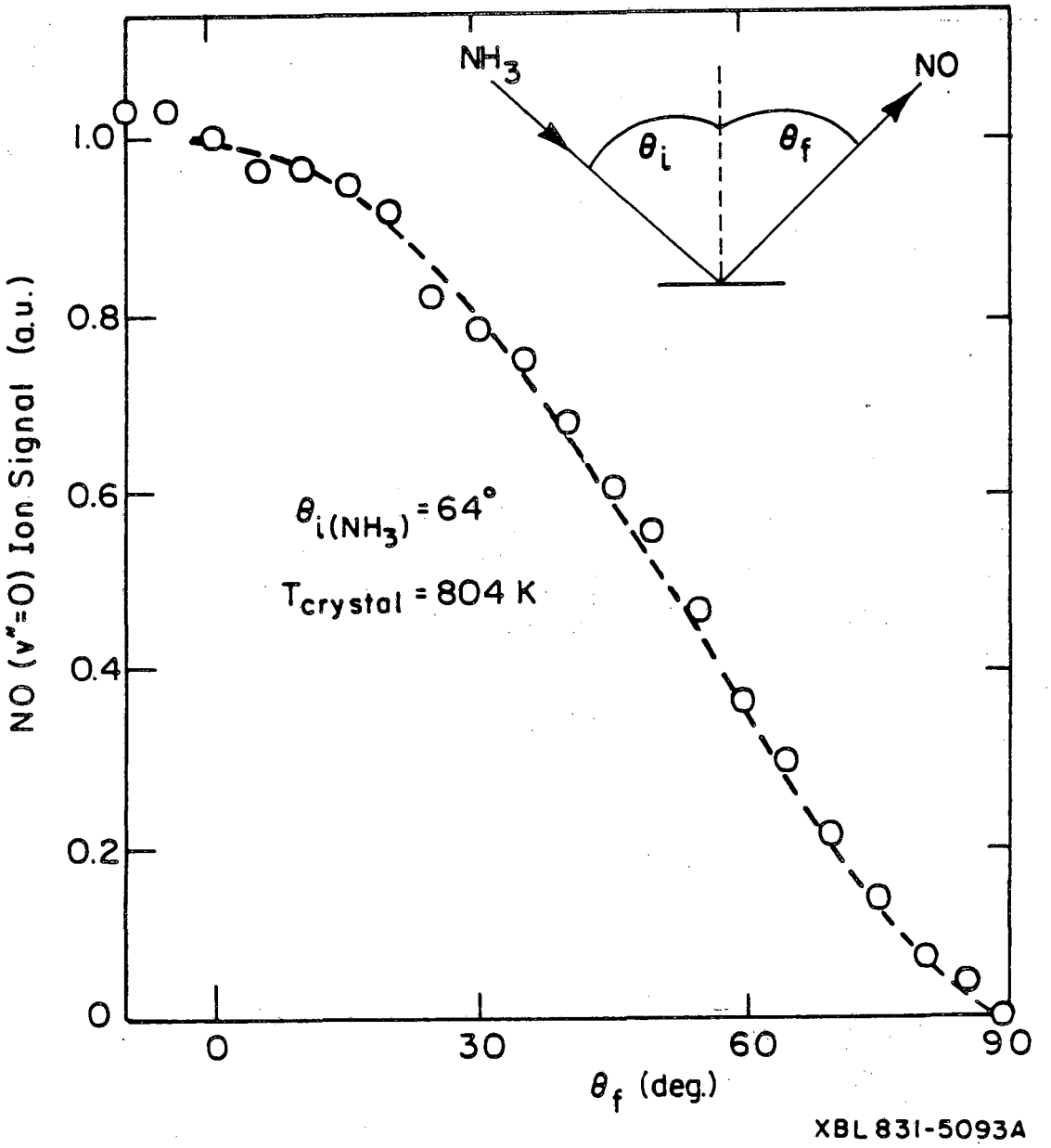
NH3
NO
θi
θf
1.0
0.8
0.6
0.4
0.2
0
NO (v"=0) Ion Signal (a.u.)
θi(NH3) = 64°
Tcrystal = 804 K
0
30
60
90
θf (deg.)
XBL 831-5093A

Fig. 21.15

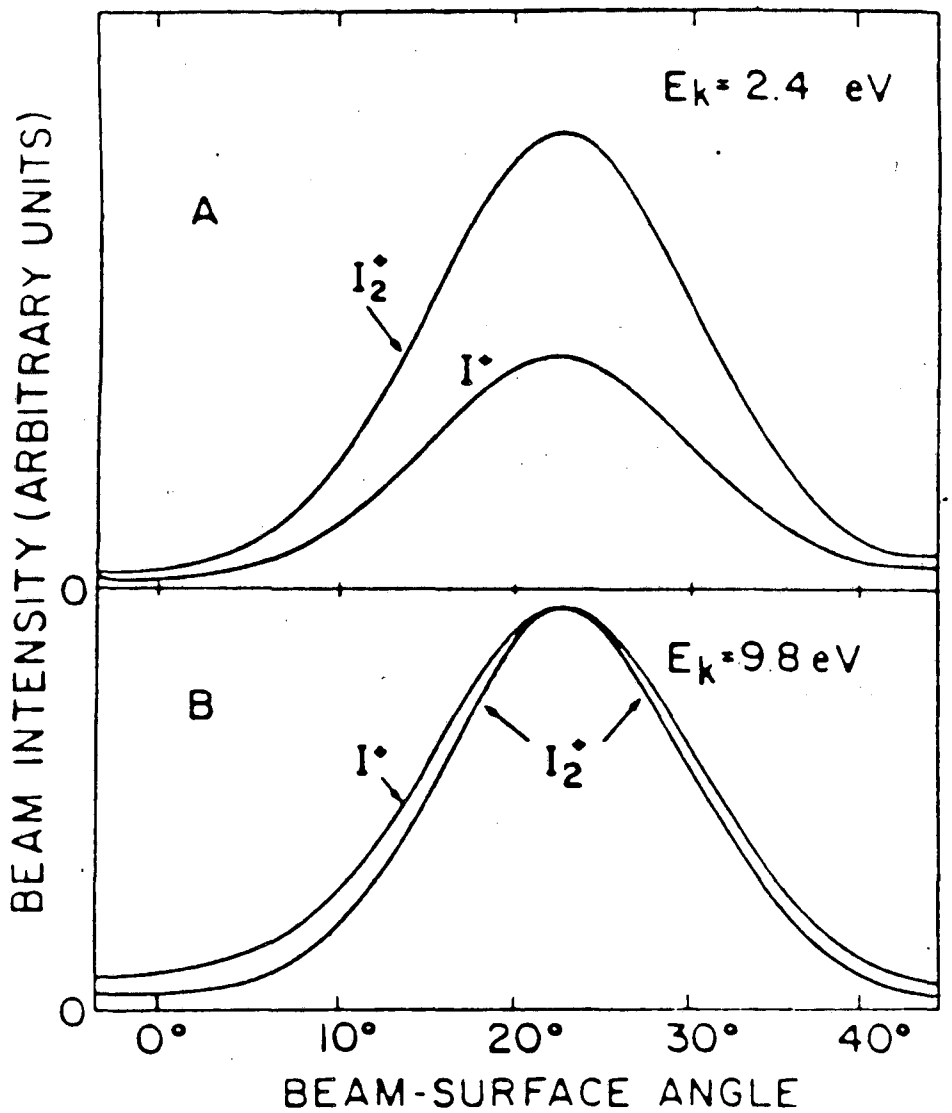
Ek = 2.4 eV
A
I2*
I*
0
Ek = 9.8 eV
B
I*
I2*
0
BEAM INTENSITY (ARBITRARY UNITS)
0°
10°
20°
30°
40°
BEAM-SURFACE ANGLE

Fig. 21.16

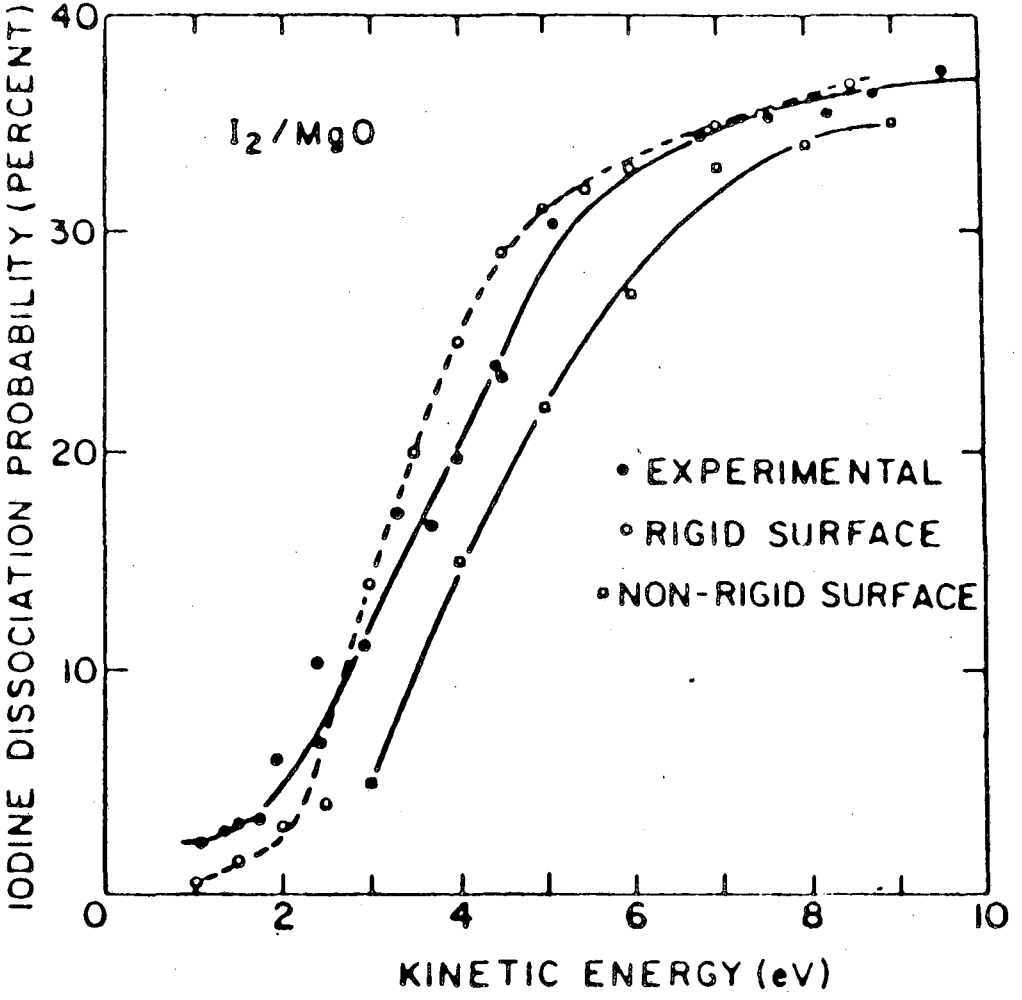
IODINE DISSOCIATION PROBABILITY (PERCENT)
40
30
20
10
0
2
4
6
8
10
KINETIC ENERGY (eV)
$I_2$/MgO
• EXPERIMENTAL
○ RIGID SURFACE
○ NON-RIGID SURFACE

Fig. 21.17

This report was done with support from the Department of Energy. Any conclusions or opinions expressed in this report represent solely those of the author(s) and not necessarily those of The Regents of the University of California, the Lawrence Berkeley Laboratory or the Department of Energy.

Reference to a company or product name does not imply approval or recommendation of the product by the University of California or the U.S. Department of Energy to the exclusion of others that may be suitable.

*LAWRENCE BERKELEY LABORATORY*
*TECHNICAL INFORMATION DEPARTMENT*
*UNIVERSITY OF CALIFORNIA*
*BERKELEY, CALIFORNIA 94720*